JOURNAL OF GEOPHYSICAL RESEARCH, VOL. 91, NO. B10, PAGES 10,355-10,382, SEPTEMBER 10, 1986

STRATIGRAPHY, PALEOMAGNETISM, AND MAGNETIC FABRIC OF THE TOBA TUFFS: CONSTRAINTS ON THE SOURCES AND ERUPTIVE STYLES

Michael D. Knight and George P. L. Walker

Hawaii Institute of Geophysics, University of Hawaii, Honolulu

Brooks B. Ellwood

Department of Geology, University of Texas at Arlington

Jimmy F. Diehl

Department of Geology and Geological Engineering, Michigan Technological University, Houghton

Abstract. The Toba depression in north central Sumatra is a complex of several overlapping calderas resulting from three major ignimbrite-forming eruptions. Within the depression, the upland masses of Samosir and northern Uluan consist of welded ignimbrite capped by coarse breccia and lacustrine sediment, hitherto interpreted to be two parts of a single resurgent dome. This study has demonstrated that the welded tuffs of Samosir and Uluan have different magnetic polarities and therefore at least two different ignimbrites are present; the Samosir/Uluan massif may consist of parts of two resurgent domes. The first ignimbrite eruption occurred at 0.84 Ma and produced a very thick (>400 m), densely welded unit having a reversed polarity. Anisotropy of magnetic susceptibility (AMS) flow direction and lithic size data indicate that the source lies in the southern part of the Toba depression, and the thick deposit of Uluan is thought to have ponded in a 40-km-wide caldera. The second ignimbrite is normally magnetized. AMS flow direction data indicate two separate source vents, one to the north in the Haranggaol caldera, and another to the south. The thick deposit at Samosir is thought to have ponded in the southern caldera. Coarse sediments then accumulated over Samosir and northern Uluan and were capped by lacustrine deposits. A renewed episode of resurgence then uplifted Samosir Island and possibly the northern part of Uluan. At approximately 0.075 Ma the last and apparently largest ignimbrite eruption occurred from calderas in the north and south parts of the Toba depression. This ignimbrite is mostly nonwelded and normally magnetized. Part of the Uluan dome was destroyed by collapse of the Sibandung caldera and Latung graben and concomitant with renewed subsidence of the Haranggaol and Porsea calderas.

Introduction

This study has used paleomagnetics to determine stratigraphic relationships between flow units along with anisotropy of magnetic susceptibility (AMS) data to determine flow direction and hence deduce source vent locations of the Toba tuff. Most samples have a well-defined AMS fabric with a maximum lineation interpreted to define a flow direction, while some have what is interpreted to be an imbrication, yielding an azimuth of flow. A pilot study has successfully correlated the χ_1 (AMS) lineation direction with the long axis direction of microscopically visible elongated crystals and lithic clasts; an extensive AMS study has constrained vent positions and yielded evidence regarding depositional and rheological conditions of the Toba ash flows.

The Toba depression measures 100 by 40 km and is associated with large-volume, thick rhyolitic ignimbrites, including intracaldera fill and thinner but very extensive and mostly nonwelded outflow sheets. Magnetic fabric and grain size distributions indicate that the ignimbrites originated from multiple vents along fissures now concealed beneath Lake Toba or beneath intracaldera fill.

Lake Toba in north central Sumatra, Indonesia (Figure 1) occupies a prominent volcanotectonic depression, first referred to by van Bemmelen [1939, 1949] as the Toba caldera. It is commonly referred to as the world's largest single caldera of Quaternary age, and from it has erupted an immense volume of rhyolitic pumice estimated at >3000 km^3 [Aldiss and Ghazali, 1984]. The topographic rim consists of often precipitous cliffs that rise 400 to 1200 m above lake level. Lake Toba is 906 m above sea level, and its maximum depth is 529 m. The depression is oval shaped and elongated NW-SE. The walls expose massively bedded ignimbrite, argillite, and limestone that are locally cut by diorite and granite. In some places the depression transects volcanoes of presumed Tertiary or Quaternary age. Inside it is a large asymmetrically rifted and apparently updomed mass measuring 55 by 25 km, constituting Samosir Island and Uluan.

A major NW-trending fault forms the western side of Lake Toba, producing a pronounced escarpment which rises 100-200 m above the eastern escarpment. A graben along the Latung Strait transects the central dome (the Latung graben [van Bemmelen, 1939]) and has precipitous walls that rise from about 400 m below lake level to a maximum elevation of 750 m above lake level on Samosir and 540 m on Uluan. Several large rivers originate in this region, but only the Asahan flows out of the lake.

Lake Toba is located in a widened portion of the Barisan Range, 100 km wide and up to 3000 m high, which forms the backbone along most of the length of Sumatra. Hamilton [1979] referred to

Paper number 5B5887.
0148-0227/86/005B-5887$05.00

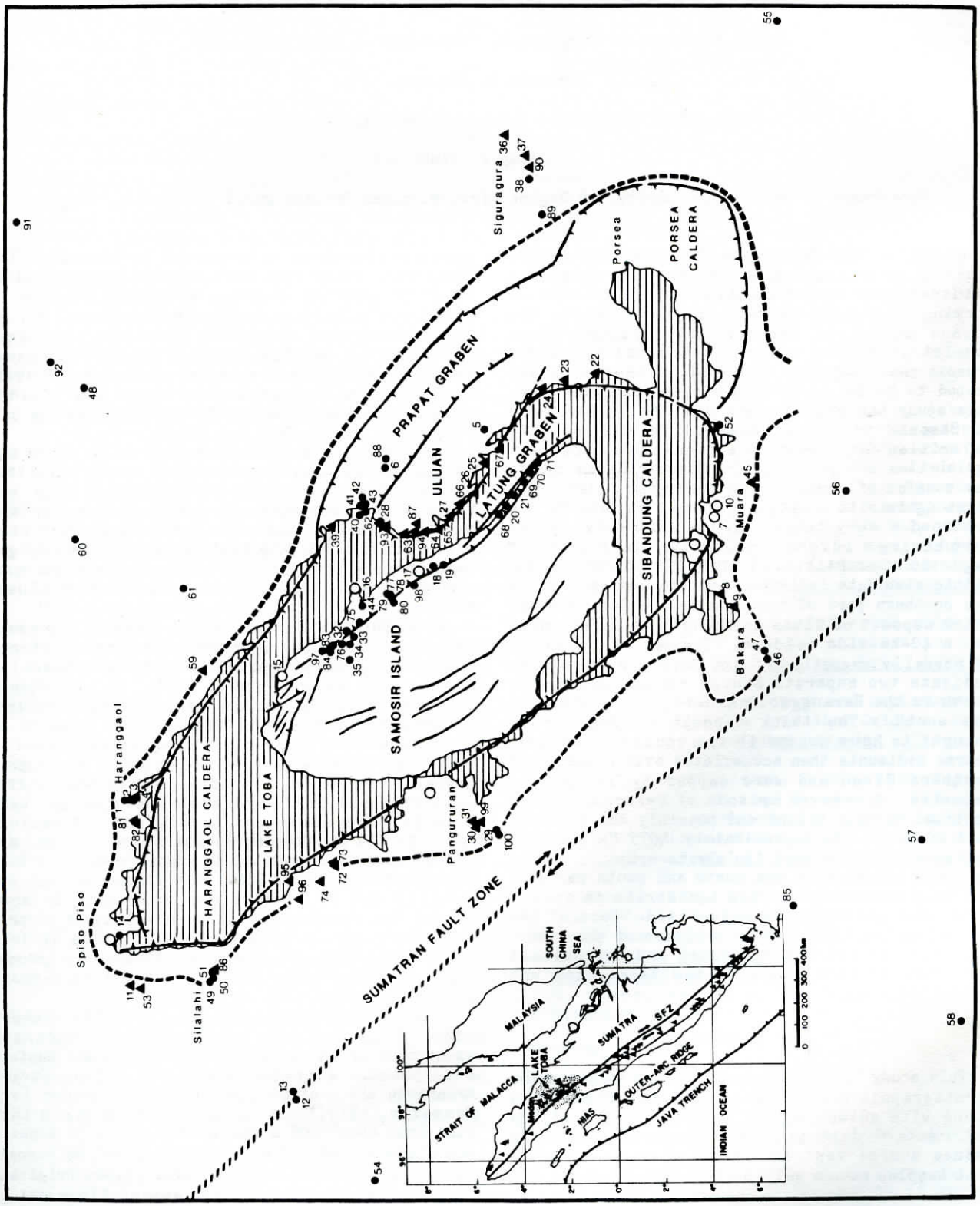
HARANGGAOL CALDERA
LAKE TOBA
SAMOSIR ISLAND
ULUAN
PRAPAT GRABEN
LATUNG GRABEN
SIBANDUNG CALDERA
PORSEA CALDERA
Porsea
Siguragura
Haranggaol
Spiso Piso
Silalahi
Pangururan
Muara
Bakara
SUMATRAN FAULT ZONE
SOUTH CHINA SEA
MALAYSIA
SUMATRA
SFZ
LAKE TOBA
STRAIT OF MALACCA
OUTER-ARC RIDGE
JAVA TRENCH
INDIAN OCEAN
NIAS
0 100 200 300 400 km

this range as a geanticline of folded Paleozoic and Mesozoic marine sedimentary and metamorphic rocks. It is surmounted by a line of Plio-Pleistocene active calc-alkaline stratovolcanoes of the Sunda Arc.

The Toba depression is elongated parallel with, and is situated 10 to 15 km east of, the Sumatran Fault Zone (SFZ), which is possibly the most important structural element in this part of Sumatra. The SFZ parallels the Sunda Trench and runs the 1650 km length of the volcanic chain. Fitch [1972] considers it to be an active transcurrent fault with major right-lateral strike-slip movement and with considerable vertical displacement near Lake Toba. The alignment of longitudinal grabens (e.g., the Prapat and Latung grabens), the elongated morphology of the Toba depression, and the resurgent domes parallel to the SFZ suggest an important genetic relationship with this major fault system.

Summary of Previous Research at Lake Toba

Van Bemmelen [1939, 1949] wrote the first comprehensive geological interpretation of the volcanotectonic history of the Toba area, in which he described the chain of events that led to the formation of the Toba caldera and subsequent formation of the Samosir Island-Uluan dome. His interpretation was that both asymmetrical half domes (Samosir forming the western flank, and Uluan forming the eastern flank), which consist of apparently identical densely welded ignimbrite, were formed by the same upheaval. Evidence for this updoming is the westward dipping (5°- 8°) lacustrine deposits capping Samosir Island, and the eastward dipping (10°- 15°) bedded tuffs capping the Uluan block. Westerveld [1947, 1952], through petrographic study, identified the welded rhyolitic tuffs as ignimbrites, macroscopically and microscopically similar to the welded rhyolitic ignimbrites of the Taupo Zone in New Zealand. We use "ignimbrite" in the sense of Sparks et al. [1973] as a pyroclastic deposit or rock body composed predominantly from pumiceous material, which may or may not be welded, and which shows evidence of having been emplaced as a concentrated hot and dry particulate flow. We use "ash flow" to denote a moving pyroclastic flow.

Gravity studies led Nishimura et al. [1977] to suggest that Lake Toba is not a single caldera but a complex of several calderas or a line of calderas, and the latest gravity map [Nishimura et al., 1984] indicates a symmetrical, low Bouguer anomaly 20 km across centered near Porsea. From the gravity anomalies associated with known calderas [Yokoyama, 1963], they inferred that a buried caldera exists at Porsea which has a mass deficiency of about 1.0×10^{11} t. Their interpretation assumes that the negative anomaly results from an infilling of low-density clastic rocks.

More recently, paleomagnetic studies have tried to unravel the stratigraphy of the Toba tuffs. Hirooka [1978] was the first to report reversed polarity natural remanent magnetization (NRM) directions for the Toba tuffs collected near Siguragura in the canyon along the Asahan River. Yokoyama et al. [1980] conducted a paleomagnetic study on 160 samples collected from 14 sites near Lake Toba and found a reversed polarity NRM for the "Haranggaol andesite" (an andesitic rheoignimbrite underlying the Toba tuffs at our locality T4), dated by Nishimura et al. [1977] at 1.2 Ma; they suggested it may have formed during the Matuyama Polarity Chron. They also found a reversed polarity for the "Tuktuk dacite" at Pangururan, which they incorrectly identified as the Tuktuk dacite on the eastern shore of Samosir which has a K-Ar age of 1.9 ±0.4 Ma and a fission track age of 2.0 ±0.3 Ma, and suggested that they both belong to the Matuyama Chron. Nishimura et al. [1984] interpreted the "Tuktuk dacite," which is a low-silica rhyolite with 72% SiO_2 (C. Chesner, written communication, 1983), as an ignimbrite that was erupted along the Sumatran Fault Zone during an earlier volcanic episode and covered a broad region of northern Sumatra.

Yokoyama et al. [1980] reported normal magnetic polarity for the upper half of the sequence of tuffs at Haranggaol, one of which yielded a fission track age of 0.07 ±0.01 Ma [Nishimura et al., 1977]. They indicate a reversed polarity Toba tuff at Haranggaol (not documented in this study) and Prapat, also fission track dated at 0.075 Ma. Hirooka [1978] reported a reversed polarity for a "Young tuff" at Siguragura from which Nishimura et al. [1977] obtained a fission track age of 0.07 Ma. Yokoyama et al. [1980] suggest that these relatively young reversed rocks belong to the Blake Event. Nishimura et al. [1984] relate the "Young Toba tuffs" to two formations (the Haranggaol and Siguragura formations) the latter having a reversed magnetic polarity and a K-Ar age of 0.075 Ma [Ninkovich et al., 1978a] and a fission track age of 0.10 ±0.02 Ma, possibly related to the Blake Event [Smith and Foster, 1969]. Chesner [1984] reports a fission track age of 0.5 Ma for the oldest Toba tuff, and Diehl et al. [1984] suggest that it was emplaced during the "Emperor" event [Ryan, 1972]. However, the 0.5-Ma-age date is now considered to be unlikely (C. Chesner, written communication, 1985). Most recently, a $^{40}Ar/^{39}Ar$ date of 0.84 Ma (T. Onstolt, oral communication, 1986) for the oldest Toba tuff seems to give the best estimate of its age, and therefore would put it in the Matuyama Chron. This date is supported by a preliminary fission track date of 0.85 Ma (C. Chesner, oral communication, 1986).

Ninkovich et al. [1978a,b] found a widespread rhyolitic ashfall deposit in deep-sea cores collected over a large part of the Indian Ocean floor, and from its chemical composition and the

Fig. 1. Map of the Toba depression showing paleomagnetic sites drilled in situ. The solid circles represent sites of welded normally magnetized ignimbrite, solid triangles are reversely magnetized, and open circles represent andesitic to rhyolitic post-Toba tuff lava domes. The location map of Sumatra (inset) shows the extent of the Toba ignimbrite outflow sheets (stippled), Quaternary stratovolcanoes along the Sunda Arc (solid triangles), and the Sumatran Fault Zone (SFZ), in relation to the Outer-Arc Ridge (accretionary prism), and the Java Trench (Sunda Trench) in which the Indian Ocean lithospheric plate is subducting obliquely to the northeast at 67 mm/yr under the Eurasian plate.

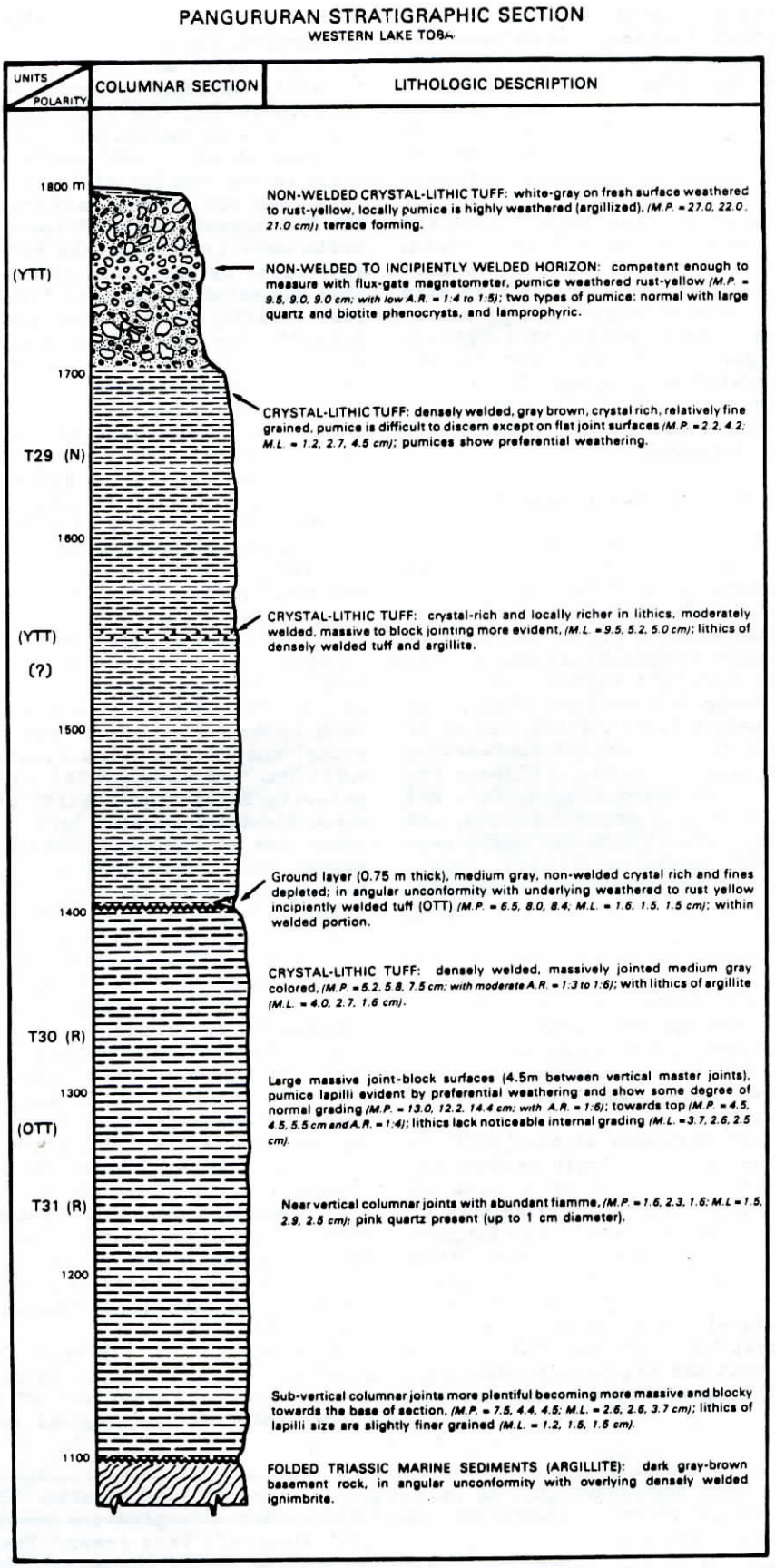

Fig. 2. Stratigraphic section at Pangururan. M.L. stands for the maximum lithic size; A.R. stands for aspect ratio; (N) stands for normally magnetized sites, and (R) stands for reversely magnetized sites. Stratigraphic elevation is given in meters.

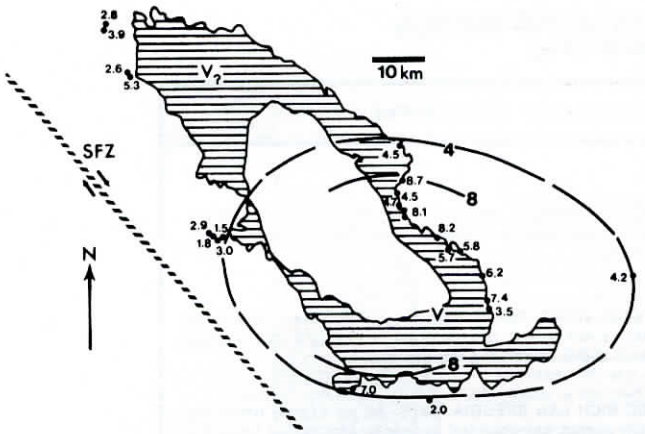

Fig. 3. Distribution of the average maximum diameter of the three largest lithic clasts in the OTT. The generalized isopleths (values in centimeters) are given, and the inferred vent(s) locality "V" is shown. The OTT at the northern end of Lake Toba is thought to have come from a different vent ($V_?$).

occurrence of allanite they correlated it with the Toba tuff. Biotite from this ashfall yielded a K-Ar age of 74.9 ± 12 x 10^3 years. Because of the extensive dispersal area of this presumed coignimbrite ash they concluded that this eruption was by far the largest in magnitude documented from the Quaternary. They estimated that the eruption column height was at least 45 km and possibly more than 50 km. Ledbetter and Sparks [1979] deduced from bedding and grading characteristics that the ash accumulated over a period of approximately two weeks.

Stratigraphy of the Toba Ignimbrites

Field observations and paleomagnetic evidence at Toba indicate that the rhyolitic Toba tuffs are ignimbrites generated by at least three major eruptions, the youngest being the thinnest, the most extensive, and the least welded [Knight, 1985]. The youngest Toba tuff is referred to as the YTT, the oldest as the OTT, and the intermediate one as the MTT. The location of each vent is discussed below.

The three Toba ignimbrites are mineralogically similar; they are high-K calc-alkaline, rhyolitic ignimbrites [Hutchinson, 1982] with 68 to 76% SiO_2 [Chesner and Rose, 1983], and are conspicuously crystal-rich (30 to 50% crystals). The phenocrysts consist of quartz, feldspar (plagioclase and sanidine), biotite, and hornblende with minor orthopyroxene, allanite, and opaques (magnetite and ilmenite) and trace amounts of zircon and apatite.

These ignimbrites are poorly sorted, massive deposits. They contain less than 5% of angular to subangular accidental lithic fragments of argillite, andesite, limestone and welded ignimbrite that range from a millimeter to nearly a meter in diameter. They lack any visible internal grading apart from a concentration of lithics towards the base of some units and a concentration of large pumice clasts towards the top of some thin flow units. Essential pumice clasts in the incipiently to nonwelded tuffs range from millimeter to meter size, are well rounded to subrounded, and tend to have lower crystal contents than the matrix. In the densely welded tuffs deformed juvenile clasts (fiamme) typically have an aspect ratio of 1:5 to 1:10.

The OTT is mostly densely welded and locally vitrophyric and rests unconformably on folded and metamorphosed marine sediments of Paleozoic and Mesozoic age (Figure 2). It is reversely magnetized, generally more than 300 m thick, it locally contains multiple flow units, and the quartz crystals in it (up to 1 cm in size) are often pink. The OTT outcrops mostly within the Toba depression and forms the rim at Pangururan, but outcrops of the outflow sheet occur at Siguragura and near Sidikalang. Cliffs with near-vertical, closely spaced prismatic to columnar cooling joints, generally 1-2 m wide and extending up to 50-75 m high, are found in the middle portion of the OTT along northern Uluan. The densely welded part of the OTT forms spectacular cliffs. Locally toward the base (e.g., at locality T22) an intensely welded, thin, dark gray-black vitrophyric layer 5-10 m thick occurs that contains abundant glassy fiamme with a well-developed eutaxitic texture. This ignimbrite contains scattered undeformed angular and often bladelike lithic fragments of argillite which are up to 3.5 cm in size.

The main outcrop of the OTT is in the south part of the Toba depression, suggesting that the main source was in that area. The distribution of the average maximum size of the three largest lithics (Figure 3), combined with grain orientation studies and AMS data, confirms this. The OTT is of high aspect ratio type and is thought to be mainly caldera fill. A crude volume estimate of 500 km^3 is based on a 40-km-wide caldera completely filled to a depth of 400 m.

The MTT is partially to densely welded, is generally between 100 m and 300 m thick, and locally contains more than 100 m of densely welded vitrophyre near its base (Figure 4). It has a normal magnetization, which distinguishes it from the OTT. The MTT is exposed mostly along the northern rim of the Toba depression at Silalahi, Spiso Piso, and Haranggaol, and on the eastern side of Samosir Island (Figures 4 and 5). A sequence of sediments about 100 m thick overlies the MTT which forms a major escarpment along eastern Samosir. They are coarse-grained breccias composed of angular to subrounded welded tuff, andesite, diorite, and the occasional limestone clasts and grade upward into medium- to fine-grained thinly laminated fluvial and lacustrine deposits less than 30 m thick. The welded ignimbrite on Samosir is more than 300 m thick (base not exposed) and could be an intracaldera deposit. There is evidence for the occurrence of another normally magnetized ignimbrite of very local extent on low ground along NE Samosir which is not overlain by the thick clastic sediments, and this is interpreted to be YTT. Dating could resolve this question.

The YTT (Figures 2 and 4) is mostly nonwelded, although locally where it is thickest (>100 m) it is incipiently to densely welded. It occurs all around the Toba depression and also at many places inside. It is normally magnetized and has similar NRM directions to that of the underlying MTT (Figures 6a-6c), thus making its distinction from the MTT somewhat problematic in welded outcrops.

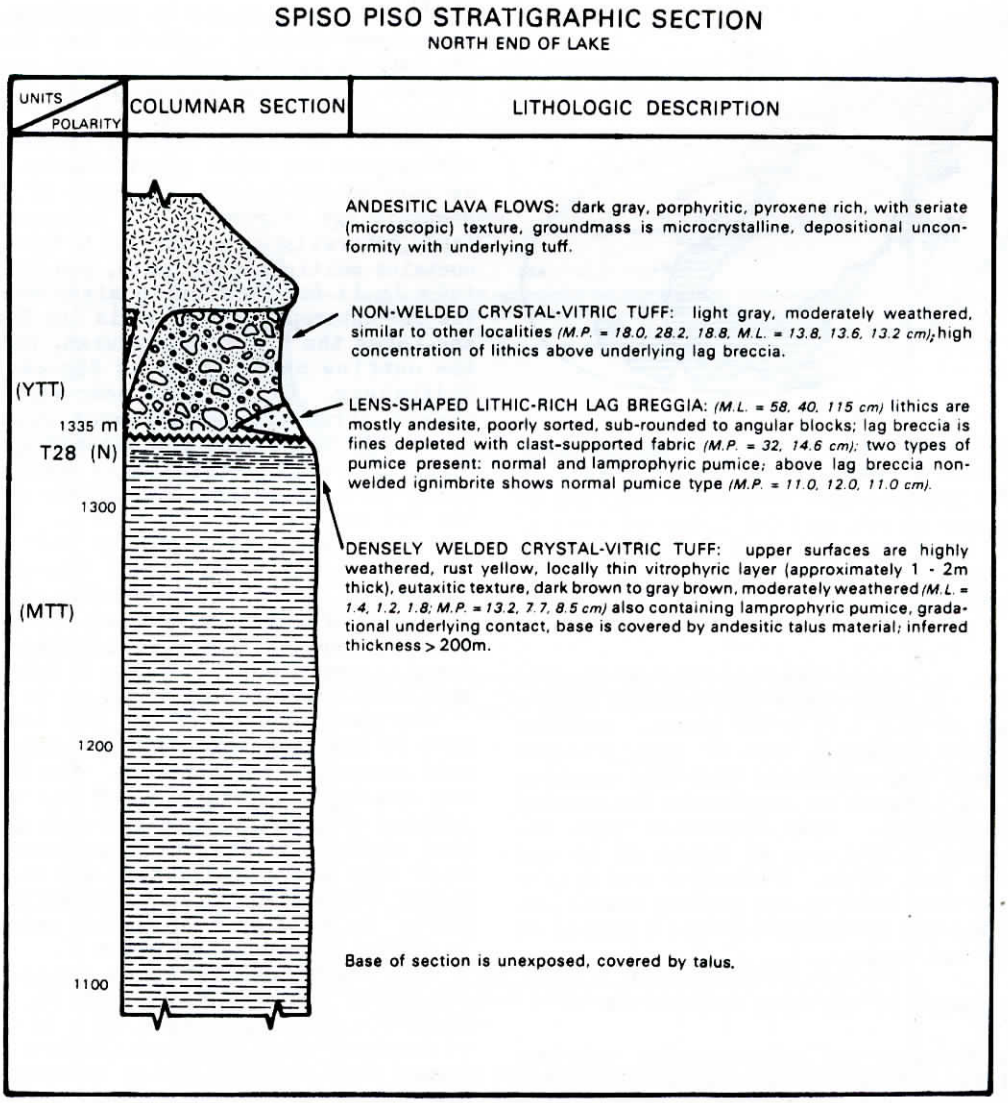

Fig. 4. Stratigraphic section at Spiso Piso.

The YTT is generally much coarser and locally contains rounded, pumice blocks up to 80 cm and lithic blocks up to 50 cm in size (Figure 5). A well-defined erosional unconformity and locally fines-depleted basal lithic-rich lag breccia and/or ground layer at the base separates the YTT from MTT (Figures 4 and 5). The lag breccia is thought to represent a proximal near-vent deposit formed within the deflation interval [Walker, 1985] and is found locally at the base of the YTT at Spiso Piso, Haranggaol, and Muara. Elsewhere a thin ground layer as first proposed by Walker et al. [1981] occurs at the base and is separated from the overlying ignimbrite by a sharp and near-planar contact. Both of these deposits are noteworthy for the strong fines depletion that they show. The Porsea caldera and a graben, referred to as the Prapat graben, are partially filled with nonwelded YTT that forms a flat terrace surface. The YTT outflow sheets form a well-developed, outward sloping (1^{o}-4^{o}) plateau that covers an estimated 20,000 km^2 of north central Sumatra.

The YTT is a moderately high aspect ratio ignimbrite that covers a remarkably wide area and has an average thickness of not less than 100 m. Its volume is at least 2000 km^3, making it the largest known ignimbrite in the Quaternary.

Paleomagnetism

Introduction

Samples for remanent and induced magnetic analyses were collected from the Toba tuffs and associated volcanic rocks during three field seasons. Thirty-five large oriented hand samples were collected in 1983 and 600 cores were drilled in situ from 100 localities (Figure 1), in 1984 and 1985 using a portable gasoline-powered rock drill and oriented by means of a Brunton and sun compass. A portable flux gate magnetometer was used in the field to seek paleomagnetic reversals within the welded tuffs. It was extremely useful in areas where no unconformity could be seen and for determining the general distribution of polarity units.

Stability of Remanent Magnetization and Rock Magnetization

The site-mean NRM directions based on 774 cores are shown in Figures 6a-6d and summarized in Table

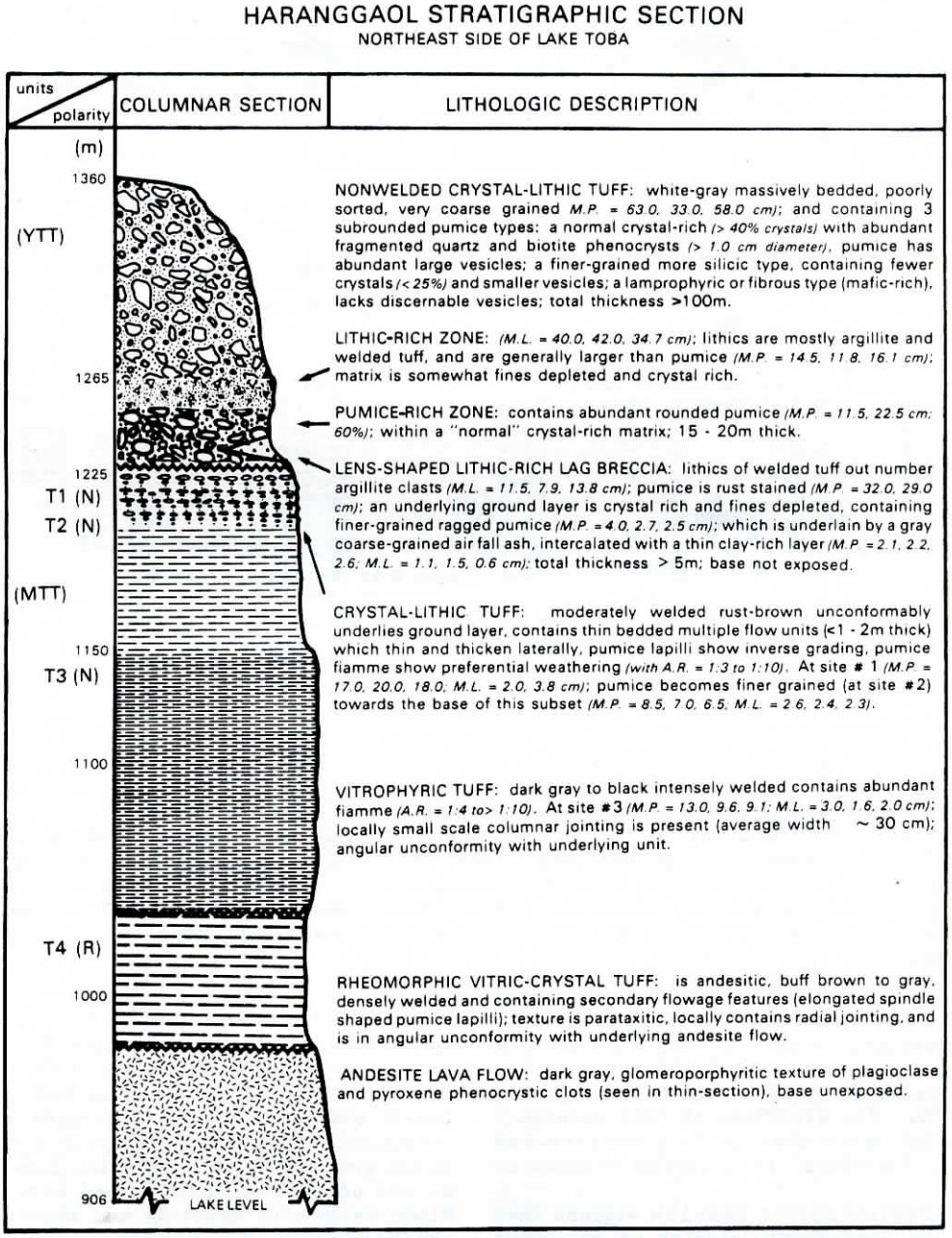

Fig. 5. Stratigraphic section at Haranggaol.

1. It was hoped that the site-mean directions for the normal polarity YTT and MTT ignimbrites might be sufficiently different so as to distinguish between the two. Both units are tightly clustered, however, and the mean declinations and inclinations are not significantly different at the 95% confidence level (Figures 6b and 6c). The site-mean direction for the reverse polarity OTT also shows a tight cluster (Figure 6d). Following NRM measurements at least two specimens from each site were demagnetized by alternating field (AF) methods in a three-axis tumbler, with magnetic induction levels to 60 mT, or by using a nontumbling custom-designed apparatus to 80 mT. An additional two samples from each site were subjected to progressive thermal demagnetization to temperatures in excess of 600°C. Both demagnetization techniques isolate the same magnetic direction from specimens cut from the same core, and these directions vary by less than 2° from the original NRM direction. Therefore, we infer that the site-mean NRM directions shown in Figures 6a-6d reliably depict the orientation of the stable magnetization for the Toba tuffs. Figures 7a-7c are representative plots that show the typical small ($\leq 10°$) changes from the NRM direction that occur with progressive AF demagnetization.

With few exceptions, orthogonal vector plots [Zijderveld, 1967] of the alternating field demagnetization display a univectorial decay to the origin indicative of a single, characteristic component of magnetization and general lack of secondary overprinting (Figure 7c). Figures 7d-7f show the thermal demagnetization behavor which

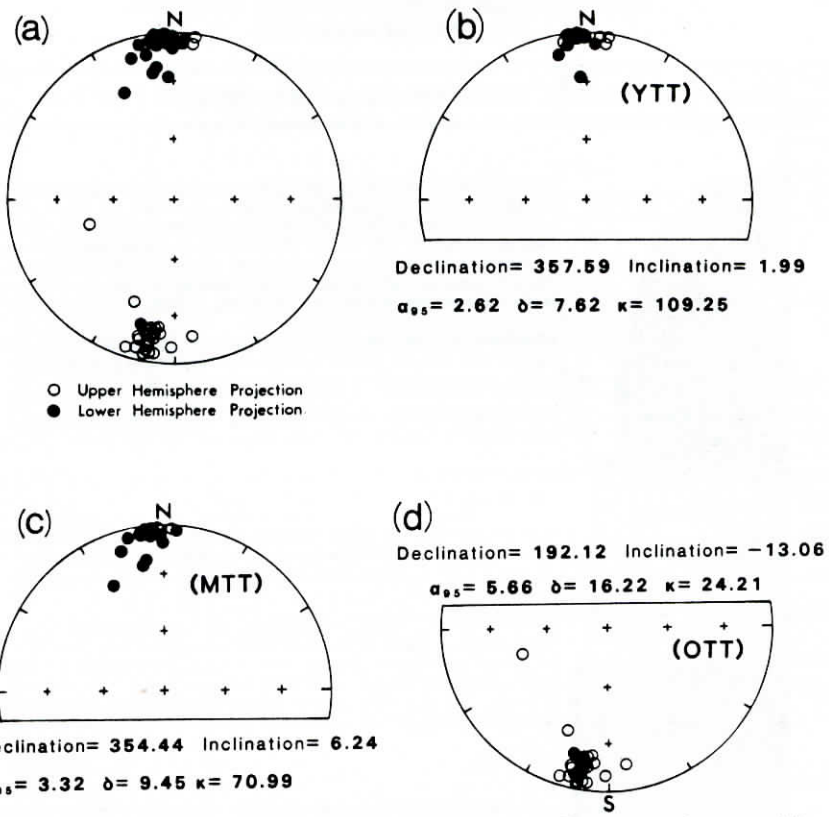

Fig. 6. (a) Equal area projection of the mean natural remanent magnetization (NRM) direction for 97 Toba tuff sites at Lake Toba. (b) Equal area projection of all YTT sites and corresponding mean declination and inclination (α_{95} and κ are as described for Table 1; δ is the angular standard deviation of the mean direction). (c) Equal area projection of all MTT sites and corresponding mean declination and inclination. (d) Equal area projection of all OTT sites and corresponding mean declination and inclination.

identifies a stable component of magnetization. Secondary magnetizations when present are easily removed by either alternating field demagnetization to peak fields of 10 nT or thermal demagnetization to 200°C. The direction of this secondary magnetization indicates that it is a present-day overprint and, therefore, is probably viscous in origin.

Thermal demagnetization results suggest that magnetite is the predominant carrier of remanence in the Toba tuffs. Thermomagnetic analysis indicates a magnetite with a Curie temperature (T_c) between 480° and 550°C. The ratio of the saturation remanence to the saturation magnetization (J_{rs}/J_s) has values that range from 0.07 to 0.24. The ratio of the remanent coercivity to the coercivity (H_{rc}/H_c) has values that range from 1.75 to 5.75. When one is plotted aganist the other, most of the samples measured (7 out of 8) fall in the pseudosingle domain region of Day et al. [1977]. Additionally, a high blocking temperature component is also present but only constitutes a small portion of the total intensity of a sample.

Fe-Ti Oxide Petrography

The Fe-Ti oxide petrography and oxidation state, and the bulk titanomagnetite content, were determined on a representative suite of Toba samples using reflected light microscopy and point counts in plain polarized light at magnifications up to x1000. The major magnetic mineral is a member of the titanomagnetite (magnetite to ulvospinel) solid solution series, generally of low-Ti content, that has undergone some degree of oxidation. Ilmenite phenocrysts are also present in the groundmass, as exsolution lamellae parallel to the octahedral plane, and within fractures. Minor amounts of hematite and maghemite were also observed, mostly along margins and within fractures of the magnetite and titanomagnetite grains and as microlites, respectively. Magnetite grains range in size from about 1.5 mm to a few microns. Microlites of homogeneous magnetite commonly occur as inclusions, along grain boundaries, and throughout the groundmass. It has been suggested [Verhoogen, 1959; Ozima and Ozima, 1965; Larson et al., 1969] that the very fine particles (<2 μm) are the probable carriers of the observed stable remanence. Supporting evidence that the groundmass titanomagnetites are the most influential carriers of remanence is suggested by the hysteresis properties of the Toba tuffs discussed previously.

Anisotropy of Magnetic Susceptibility

Introduction

An inherent problem in the investigation of every ignimbrite is the determination of its

TABLE 1. Mean NRM Directions of the Toba Tuffs

Locality	Unit	Declination	Inclination	N	κ	α_{95}
		Normal Polarity Sites (YTT, MTT)				
T-1	MTT	354.32	2.67	8	400.5	1.8
T-2	MTT	358.53	6.50	7	433.4	1.9
T-3	MTT	4.61	3.46	9	150.7	2.4
T-5	YTT	353.03	1.44	6	180.1	4.3
T-6	YTT	3.33	7.72	8	5.1	16.1
T-12	YTT	359.18	3.71	8	232.1	3.1
T-13	YTT	357.12	2.12	7	153.8	4.3
T-14	MTT	2.85	-2.36	7	63.1	6.7
T-18	MTT	353.37	2.62	8	727.8	1.8
T-19	MTT	354.53	2.03	8	330.3	2.7
T-20	MTT	356.20	2.58	4	116.0	6.5
T-21	MTT	353.25	2.65	4	655.9	2.7
T-29	YTT (?)	355.20	-2.47	6	94.5	5.9
T-32	MTT	351.07	3.28	8	259.8	3.1
T-33	MTT	352.36	21.42	8	188.1	3.6
T-38	YTT	358.36	3.80	7	278.4	3.2
T-40	YTT	357.24	1.42	7	224.5	2.7
T-41	YTT	7.73	-2.63	7	26.5	7.3
T-42	MTT (?)	355.79	2.78	7	645.3	1.5
T-43	MTT (?)	334.83	30.38	5	6.5	24.6
T-44	YTT	353.78	0.57	8	89.1	5.2
T-46	YTT	357.23	27.69	9	78.2	4.4
T-47	YTT	353.18	8.32	8	727.4	2.0
T-48	YTT	356.95	1.62	5	73.4	8.5
T-49	YTT	348.95	13.28	7	262.3	3.3
T-50	MTT (?)	359.46	11.18	7	205.1	3.7
T-51	MTT (?)	356.71	3.11	7	361.8	2.8
T-52	YTT	7.10	-7.13	5	70.4	7.5
T-54	YTT	355.46	0.68	15	655.7	1.4
T-55	YTT	358.50	-1.83	21	180.2	2.3
T-56	YTT	357.01	0.12	8	107.6	4.8
T-57	YTT	359.35	1.46	18	125.5	2.9
T-58	YTT	355.68	3.02	16	104.9	3.4
T-60	YTT	355.60	3.53	16	184.2	2.6
T-61	YTT	358.37	2.05	6	829.6	2.0
T-62	YTT (?)	4.81	-2.52	10	173.6	3.4
T-68	MTT	357.85	-1.37	6	1654.4	1.4
T-69	MTT	354.90	1.20	16	608.5	1.4
T-70	MTT	353.94	6.17	11	805.9	1.5
T-71	MTT	352.94	-1.43	11	145.1	3.5
T-75	MTT	359.34	3.24	17	324.6	1.9
T-76	MTT	343.07	12.99	12	90.5	4.2
T-77	MTT	354.52	0.82	15	143.8	3.0
T-78	MTT	357.40	5.57	7	287.0	3.1
T-79	MTT	359.54	6.23	9	143.0	3.9
T-80	MTT	347.06	5.90	9	57.9	6.1
T-83	MTT	351.86	5.70	18	131.7	2.9
T-84	MTT	350.75	24.47	14	16.7	9.2
T-85	YTT	356.50	1.64	8	214.6	3.4
T-88	YTT	356.49	-3.88	5	41.5	9.7
T-89	YTT	359.72	-3.11	9	76.0	5.4
T-91	YTT	351.44	-5.34	7	80.4	5.9
T-92	YTT	356.94	-0.45	11	104.8	4.1
T-97	MTT	355.10	7.06	14	182.4	2.8
T-100	YTT (?)	358.24	1.46	8	167.6	3.8
		Reverse Polarity Sites				
T-8	OTT	195.49	-15.18	7	142.7	3.1
T-9	OTT	198.60	-6.30	8	180.7	3.7
T-11	OTT	191.13	-13.52	8	124.6	4.4
T-22	OTT	195.52	22.53	9	97.4	4.7
T-23	OTT	190.14	-13.37	7	738.9	1.9

TABLE 1 (continued)

Locality	Unit	Declination	Inclination	N	κ	α_{95}
		Reverse Polarity Sites (continued)				
T-24	OTT	190.16	-11.18	7	1030.1	1.6
T-25	OTT	188.02	-6.09	7	294.7	3.1
T-26	OTT	188.51	-22.29	7	22.7	11.1
T-27	OTT	187.41	-23.28	4	49.2	10.0
T-30	OTT	195.29	-7.85	8	465.4	2.3
T-31	OTT	191.92	-3.99	7	106.8	5.1
T-36	OTT	191.27	-8.40	8	650.2	1.9
T-37	OTT	189.78	-5.87	7	596.5	2.2
T-39	OTT	192.64	-7.90	8	17.5	11.8
T-45	OTT	191.71	-5.44	5	228.4	3.9
T-53	OTT (?)	253.62	-45.29	12	7.0	15.2
T-63	OTT	191.87	15.16	13	67.9	4.7
T-64	OTT	191.74	-20.05	16	579.3	1.5
T-65	OTT	190.80	-22.20	11	51.1	5.9
T-66	OTT	186.01	-18.92	10	566.2	1.8
T-67	OTT	192.69	-18.04	14	81.8	4.1
T-74	OTT	194.74	-14.03	8	36.4	8.2
T-86	OTT (?)	181.57	-11.20	9	104.8	4.6
T-87	OTT	188.68	-15.46	15	328.5	2.0
T-93	OTT	189.22	-17.86	15	1148.2	1.1
T-94	OTT	191.64	-10.91	12	757.9	1.5
T-96	OTT (?)	172.81	-17.59	15	146.3	3.0
T-99	OTT	201.67	-33.74	10	231.3	2.9

Mean paleomagnetic (NRM) direction of the Lake Toba ignimbrites drilled in situ during 1984 and 1985: N is the number of cores per site; κ is the precision parameter of Fisher [1953]; α_{95} is the radius of the cone of 95% confidence about the mean, in degrees.

source vent location. Where an ignimbrite is associated with a caldera, it is generally thought that the ignimbrite source lies within the caldera. Curtis [1955] demonstrated, however, that the Valley of Ten Thousand Smokes (VTTS) ignimbrite did not flow from a vent within the Katmai caldera and deduced that it came from a source vent at or near Novarupta.

At Towada, Kuno et al. [1964] demonstrated that the maximum lithic size and also (less clearly) the maximum pumice size in the ignimbrite decrease systematically outward from the caldera and thus provide evidence that the source lies in the caldera. Similar relations were found by Yokoyama [1974] for the Ito ignimbrite, by Sparks [1975, 1976] for ignimbrites at Vulsini, by Barberi et al. [1978] for the Campanian tuff, by Walker et al. [1981] for the youngest ignimbrite at Rabaul, and by Walker and Wilson [1983] and Wilson and Walker [1985] for the Taupo ignimbrite. Lipman [1967] found evidence for density sorting of phenocrysts and ash, resulting in systematic modal variations with distance from the Aso caldera, and systematic variations in crystal content were also found by Walker et al. [1981] at Taupo. Coarse lithic (lag) breccias from Acatlan, Mexico, were found within a few kilometers of the source vent by Wright and Walker [1977, 1981]. Lag breccias have been found elsewhere, for example at La Primavera [Wright, 1981], Santorini [Druitt and Sparks, 1982], Crater Lake [Bacon, 1983], and Aira caldera [Aramaki, 1984] and have been used to constrain source vent locations.

Other methods are required to pinpoint more accurately the source and determine whether there was a single vent or multiple vent system, and whether the latter lies on a straight fissure or on a ring fracture. One approach is to identify the accidental lithic types present in the ignimbrite [Hildreth and Mahood, 1984]. Other approaches are to determine the flow direction of the ignimbrite by studying the orientation of microscopic features such as elongate crystals and lithic fragments [Elston and Smith, 1970; Rhodes and Smith, 1972; Chapin and Lowell, 1979; Suzuki and Ui, 1982], the orientation of megascopic features such as elongated pumice clasts [Schmincke and Swanson, 1967] and entrained tree logs [Froggatt et al., 1981], or by using magnetic anisotropy [Ellwood, 1982; Incoronato et al., 1983].

The flow azimuth can be determined by imbrication of crystals, elongated pumice or other fragments [Mimura and MacLeod, 1978; Kamata and Mimura, 1983], entrained tree logs, and features such as the orientation of soil flaps attached to roots of overturned trees. Suzuki and Ui [1982] used microstructures and depositional ramp structures to delineate flow azimuth. Folding, where the axial planes dip sourceward [Schmincke and Swanson, 1967], has been shown to indicate secondary flowage down depositional slopes and not primary flow directions [Chapin and Lowell, 1979].

Previous AMS Studies

According to Rees [1965], Ellwood and Abrams [1982], and Ellwood [1984], the directions of the

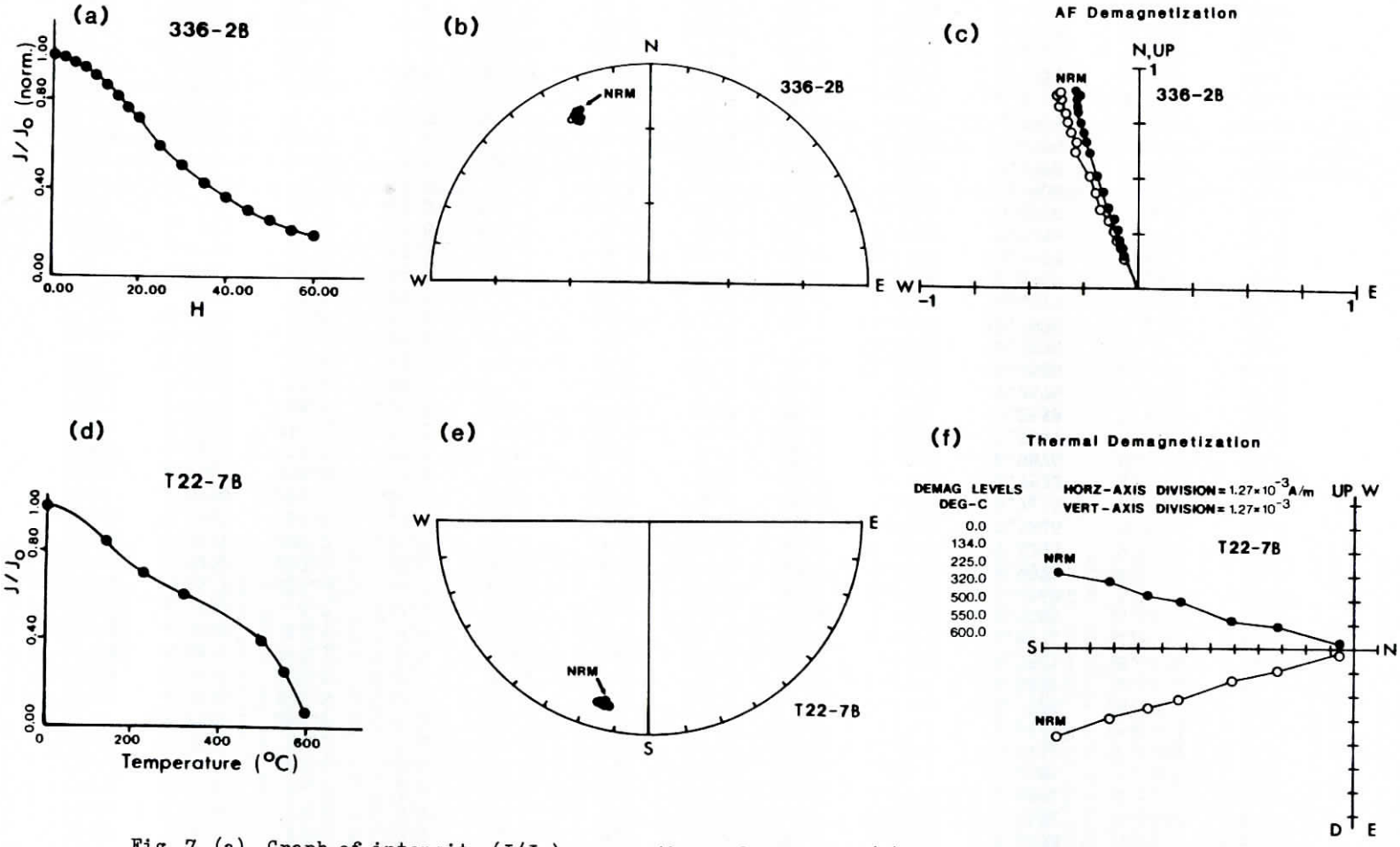

Fig. 7. (a) Graph of intensity (J/J_o) versus the applied field (H) during progressive alternating field demagnetization of sample 336-2B. (b) Equal area projection of the AF demagnetization directions; note the $<10^o$ change from the NRM direction for sample 336-2B (open circles are inclinations plotted on the upper hemisphere). (c) Vector plot of progressive AF demagnetization of sample T336-2B. (d) Graph of intensity versus the applied field during thermal demagnetization of sample T22-7B. (e) Equal area projection of the thermal demagnetization directions for sample T22-7B (solid circles represent inclinations on the lower hemisphere). (f) Vector plot of progressive thermal demagnetization for sample T22-7B.

TABLE 2. Anisotropy of Magnetic Susceptibility Data Determined From Welded Ignimbrite Along NE Samosir and SW Uluan

Sample	$\chi \times 10^{-4}$	χ_1		χ_2		χ_3		$\chi_1 \times 10^{-4}$	$\chi_2 \times 10^{-4}$	$\chi_3 \times 10^{-4}$	V
		D_{max}	I_{max}	D_{int}	I_{int}	D_{min}	I_{min}				
3091	5.7362	43.5	-23.2	140.9	-16.6	83.2	60.9	5.8755	5.7596	5.5730	51.8
3092B	6.5495	33.2	-18.9	132.2	-24.6	89.8	58.1	6.6637	6.5565	6.4282	47.6
3093B	6.6114	4.4	-15.5	109.6	-43.5	79.7	42.4	6.7378	6.6602	6.4361	59.5
3162B	3.9072	33.7	12.2	124.3	3.0	47.8	-77.4	4.0030	3.9298	3.7915	54.0
3161A	2.5273	57.2	7.2I	147.4	1.3	62.2	-82.7	2.5928	2.5384	2.4508	51.8
3161B	2.6290	56.7	2.9	146.8	0.7	70.0	-87.0	2.7165	2.6294	2.5410	45.2
3351A	5.4198	323.4	46.6	232.2	1.1	321.2	-43.4	5.4813	5.4385	5.3395	56.7
3351B	6.1897	62.0	3.4	150.9	-16.9	342.9	-72.8	6.2655	6.2154	6.0882	56.7
3352	5.8449	294.9	-1.2	204.7	-8.2	33.1	-81.7	5.9145	5.8541	5.7662	50.3
3371B	8.6923	304.6	52.7	132.7	37.0	39.8	3.9	8.8115	8.7722	8.4934	69.4
3372A	6.5955	289.5	-7.7	93.9	-82.0	19.2	2.1	6.7103	6.6287	6.4474	56.1
3373B	8.8815	310.3	5.6	139.2	84.3	40.4	0.9	8.9966	8.9501	8.6979	66.8
3381A	4.9468	14.5	1.8	103.3	-32.9	287.2	-57.0	5.1078	4.8774	4.8551	17.3
3382A	4.5490	0.7	-11.9	94.9	-19.5	61.0	66.9	4.6916	4.5085	4.4469	30.1
3382B	6.4522	352.4	-6.5	262.9	4.3	26.3	82.1	6.5883	6.4068	6.3615	26.5
3413	8.8912	287.9	-39.0	194.2	-4.6	278.5	50.6	9.0545	8.9972	8.6218	68.7
3411B	9.3411	280.2	-37.7	189.4	-1.0	278.1	52.3	9.5319	9.4293	9.0622	62.1
3414B	9.3951	67.2	41.0	170.5	14.8	276.0	45.3	9.5555	9.5246	9.1051	74.8
3481	6.6936	289.3	-20.9	194.2	-13.0	74.5	-65.1	6.8272	6.7413	6.5121	58.5
3482A	4.6993	358.9	9.8	96.0	35.7	75.9	-52.6	4.7700	4.7532	4.5746	72.9
3482B	6.9482	78.7	37.1	166.2	-3.3	71.9	-52.7	7.0533	6.9876	6.8036	59.1
3501A	5.5532	317.4	-17.0	217.8	-28.7	74.1	-55.8	5.6161	5.5811	5.4624	61.5
3501B	7.2664	288.9	-27.6	193.1	-11.0	83.5	-59.9	7.3551	7.2558	7.1884	39.5
3502B	7.2496	85.4	23.0	171.8	-8.4	63.1	-65.3	7.4056	7.2576	7.0856	47.2
3542	12.8020	42.0	49.5	189.8	35.8	292.0	16.3	12.9360	12.8580	12.6110	60.7
3544B	12.6230	72.1	81.8	245.2	8.1	335.3	1.0	12.8000	12.5830	12.4870	33.6
3543B	12.8220	35.9	-57.6	260.6	-24.3	341.1	20.1	13.0030	12.7870	12.6760	35.6
3551B	4.4208	0.0	20.1	0.0	23.8	0.0	-69.9	4.5053	4.4739	4.2833	67.9
3553	4.5207	312.6	19.9	228.2	-15.2	353.0	-64.6	4.6048	4.5767	4.3806	69.3
3602A	3.0736	21.2	10.3	110.2	-5.5	352.6	-78.3	3.1329	3.1107	2.9773	67.8
3603B	3.1453	13.9	7.6	105.0	7.6	59.5	-79.2	3.1956	3.1256	3.1145	21.7
3604	3.2151	43.7	-24.0	100.5	50.9	327.8	28.8	3.3006	3.2020	3.1426	37.8
3611	3.2495	7.0	23.2	93.3	-8.6	344.4	-65.1	3.3039	3.2606	3.1841	53.0
3612	3.2796	56.9	9.0	146.0	-5.8	23.4	-79.2	3.3541	3.3312	3.1536	70.2
3613A	3.3945	297.8	11.4	211.1	-15.0	353.4	-70.4	3.4639	3.4199	3.2997	58.8
3662B	4.8248	15.5	-15.3	105.5	0.0	15.5	74.7	4.9337	4.8979	4.6427	69.5
3663A	4.0186	24.2	-8.7	113.7	2.9	5.4	80.8	4.1199	4.0749	3.8609	65.4
3663B	5.0254	350.9	-15.7	261.9	3.5	4.2	73.9	5.1528	5.1094	4.8141	69.0
3681	8.4032	340.0	1.8	250.3	-11.6	61.1	-78.3	8.5080	8.4440	8.2576	59.6
3683	3.9099	80.5	16.5	171.6	3.6	273.6	73.1	3.9469	3.9225	3.8602	58.0
3685	5.0723	350.0	-3.6	259.7	-3.7	303.7	84.8	5.1706	5.0974	4.9488	54.9

3691B	8.5844	332.4	-9.7	238.6	-20.8	86.0	-66.9	8.8070	8.6522	8.2939	56.7
3692	8.4589	321.4	-12.7	225.9	-23.0	78.1	-63.4	8.6237	8.5670	8.1859	68.9
3693A	6.5574	333.3	-6.5	240.3	-24.7	77.0	-64.3	6.7699	6.5238	6.3786	37.5
3701B	3.7101	310.4	3.9	222.8	-32.6	34.4	-57.1	3.7835	3.7395	3.6072	60.0
3702B	2.9923	338.9	18.1	256.0	-20.7	31.2	-61.9	3.0402	3.0233	2.9133	68.6
3703B	2.5750	302.2	3.5	213.9	-25.4	25.0	-64.4	2.6329	2.5891	2.5031	54.5

AMS data for oriented block samples collected during 1983 and measured at UCSC: χ is the mass susceptibility in SI units; Dmax and Imax, Dint and Iint, and Dmin and Imin are the declination and inclination of the maximum, intermediate, and minimum susceptibility directions, respectively; χ_1, χ_2, and χ_3 are the maximum, intermediate, and minimum susceptibility magnitudes in SI units; V of Graham [1966] as defined in the text, in degrees.

AMS principal axes (χ_1- maximum; χ_3- minimum) in rocks are mainly controlled by the following factors: (1) χ_3 is aligned normal to the plane of bedding or foliation in the rock (i.e., at the pole to foliation); (2) χ_3 is aligned parallel to the axis of maximum compression (in welded ignimbrites this would be parallel to the axis of maximum compaction); (3) χ_1 for turbulent or laminar particulate flow is generally aligned parallel to the direction of flow; (4) χ_1 is parallel to lineations in the rock and lies in the foliation plane; and (5) χ_1 is aligned normal to the direction of maximum compression and parallel to the direction of maximum extension.

For ignimbrites, alignment of the AMS axes may result from laminar flowage during and after emplacement, gravitational settling of particles, and postemplacement stresses accompanying compaction, welding, and tilting.

At present, only one previous study has applied the AMS technique to ignimbrites. Ellwood [1982] employed AMS to identify source vents of welded ignimbrites associated with calderas in the San Juan Mountains. He concluded that flow direction estimates for individual sites obtained from the site-mean χ_1 were geologically reasonable, implying that linear magnetic elements in the flow were parallel to the flow direction.

Incoronato et al. [1983] studied a pyroclastic surge deposit from the Phlegrean Fields and found a close similarity to the fabric of water-laid sediments. They concluded that the depositional conditions must also be similar. Furthermore, they found that the magnetic fabric at the bottom of the deposit showed the effect of the underlying surface, whereas that near the top showed a greater influence of current flow, implying that laminar flow may have predominated immediately before deposition.

An inherent assumption in studying ignimbrites by the AMS method, is that the magnetic minerals were already present in the ashflow and did not form during postemplacement crystallization. Three lines of evidence at Lake Toba support this assumption.

1. The magnetic fabric does show a clear lineation. If the magnetic minerals were mainly formed after emplacement (e.g., during compaction and welding), then the magnetic fabric would have only a foliation or might even be isotropic.

2. Phenocrysts of mafic minerals such as biotite, hornblende, and orthopyroxene commonly enclose microlites of magnetite which were apparently present when the mafic silicates formed; the larger microlites are euhedral to subhedral.

3. Rhyolites and andesites, in general, often contain oxide pseudomorphs after mafic materials, but such pseudomorphs were not observed to be a significant component in any of the thin sections examined of the Toba welded tuffs.

AMS Methods

Anisotropy of magnetic susceptibility (AMS) refers to the variation of magnetic susceptibility with direction in a rock and can be expressed by defining three principal orthogonal axes of the maximum, intermediate, and minimum susceptibility [Nye, 1969]. The magnitudes and azimuths of these principal axes can then be related to the petrofabric of the sample. In most cases, AMS is

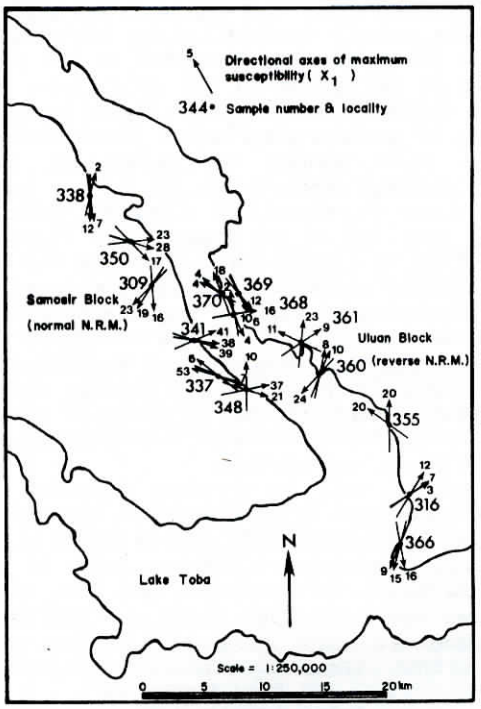

Fig. 8. AMS measurements of samples of welded ignimbrite collected in 1983 along either side of the Latung Straits. Three samples at each site were measured for AMS. The lines with arrowheads represent the plunge direction of the maximum susceptibility axis (χ_1). Arrowheads indicate the plunge in the positive (downward) direction of the χ_1 lineation direction. Dips of 30° or less in the magnetic fabric, and dips toward the Toba depression, are thought to represent imbrication of the microscopic magnetic grains and are interpreted as indicators of the flow direction, which was opposite to that shown by the arrowheads.

caused by the preferential alignment of elongated (prolate) and/or flattened (oblate) magnetic grains by processes such as laminar flowage. Since nonequant grains are most easily magnetized parallel to their longest dimension, an AMS may thus result.

Magnetic susceptibility is commonly quoted in terms of susceptibility per unit volume or mass (K or χ, respectively). In this study it was only possible (without destroying individual specimens) to measure the mass of the specimen cores rather than the volume; AMS is therefore given below in terms of mass. Mass susceptibility χ is represented by

$$\bar{\chi} = (\chi_1 + \chi_2 + \chi_3)/3 \qquad (1)$$

where (χ_1), (χ_2), and (χ_3) correspond to the maximum, intermediate, and minimum susceptibility magnitudes. Taira and Lienert [1979] have shown that for most rocks the total principal susceptibility ratios express the preferred alignment of included ferromagnetic mineral grains.

The AMS was measured, using the low-field torsion fiber magnetometer (torquemeter) basically similar to the one described by King and Rees [1962] and Stone [1963], at the University of California at Santa Cruz (UCSC) and the University of Texas at Arlington (UTA). Another suite of samples was subsequently measured at the University of Hawaii (UH) using a balanced bridge spinner, similar to the one described by Graham [1967].

Samples were oriented cylindrical cores ~2.5 cm in diameter and length. Longer cores were cut into two or three samples and labeled A, B, and C, where A is the lowest and generally least weathered and B or C the top.

Only three samples per site collected in 1983 were measured for the preliminary AMS study at UCSC (47 samples total, Table 2), so there was no statistical criterion for eliminating any sample that might be anomalous to a particular locality. Therefore, only the maximum susceptibility (χ_1) for each sample at these sites is reported in Figure 8. AMS study of 549 samples of welded ignimbrites collected in 1984 and 1985 was conducted at UTA and UH. This large data set, averaging six samples per site, provided enough sample data for calculating the AMS mean principal directions. The results are presented in the following section.

The total anisotropy (H) has been represented by the equation [Owens, 1974]

$$H = (\chi_1 - \chi_3)/\bar{\chi} \times 100 \qquad (2)$$

A plot of H versus V for 549 AMS measurements is shown in Figure 9. The mean value of H of 4.3% is well within the experimental precision of the torquemeter [Ellwood, 1984]. An anisotropy of more than 10% may influence the directions of remanent magnetization [Uyeda et al., 1963], and only 20 samples exceeded this value.

The parameter V [Graham, 1966; Figure 9 and Table 3] is a convenient index of shape and ranges in value from 0°- 44° for a prolate ellipsoid to 46°- 90° for an oblate ellipsoid. V is given by the following relationship

$$\sin^2 V = (\chi_2 - \chi_3)/(\chi_1 - \chi_3) \qquad (3)$$

In Figure 9, 29% of the samples fall in the prolate region. Graham [1966] used V to differentiate between primary versus secondary magnetic fabric and suggested that V should be greater than 45° for undisturbed sediments. Nearly three-fourths of the Toba samples exhibit V greater than 45° and are thus inferred to have a primary magnetic fabric (Figure 9).

Another type of two-axis ratio plot used to classify the shape of individual grains and describe the form of the AMS ellipsoid, following the convention of Flinn [1962] for strain ellipsoids, is shown in Figure 10 and plots the ratio χ_1/χ_2 against the ratio of χ_2/χ_3. Of the 538 samples plotted, 26% fall in the prolate ellipsoid field similar to the results based on Graham's V; therefore the Toba samples are dominated by oblate grains.

A useful quantitative measure of the lineation (l) and foliation (f) was given by Khan [1962], where

$$l = (\chi_1 - \chi_2)/\bar{\chi} \qquad (4)$$

$$f = (\chi_2 - \chi_3)/\bar{\chi}. \qquad (5)$$

As shown in Table 3, l is less than f at 72 sites,

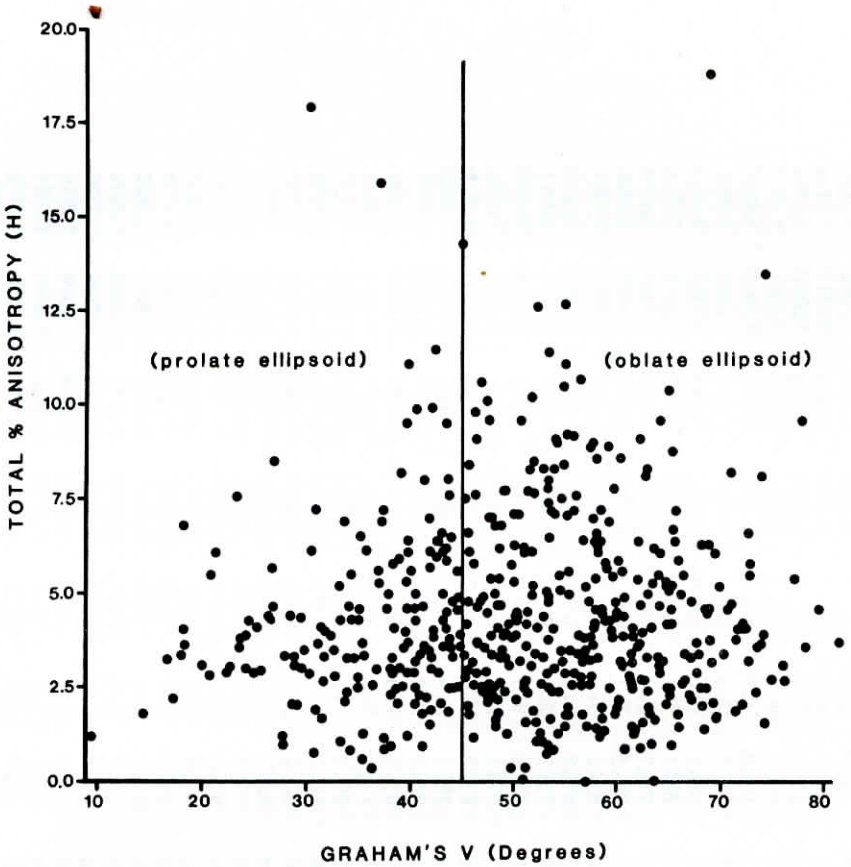

Fig. 9. Two-axis plot of Graham's V (in degrees) versus the total percent anisotropy "H" (as defined in the text) for 538 samples. "H" ranges from 0% to greater than 18%. The Graham's V values are separated into two fields, represented by samples that contain grains whose shapes are dominated by prolate ellipsoids (cigar-shaped) or samples which tend to be dominated more by oblate ellipsoids (flattened pancakes). Twenty-five percent of the samples measured fall within the prolate field and are therefore dominated by elongated magnetic grains, while a majority of the samples (75 %) must be dominated by oblate-shaped ones.

implying that the individual grains tend to resemble oblate ellipsoids or that random orientation of prolate grains in the bedding plane is much higher than at right angles to it. These results are similar to those described by Taira and Lienert [1979] for the Salton Sea dunes. Good lineation directions ($l > f$) are inferred for 13 of the sampled sites, suggesting that grain shape is also dominated by prolate ellipsoids at some localities (Table 3).

Summary of AMS Measurements

AMS equal-area lower hemisphere plots of χ_1, χ_2, and χ_3 in general show that χ_3 is usually well grouped in the vertical direction, perpendicular to the foliation containing χ_1 and χ_2. A representative suite of the AMS plots for the 72 sampled sites in and around Lake Toba is presented in Figure 11 and is grouped into the following four categories; (1) good clustering of χ_3 near vertical along with good clustering of χ_1 in the foliation plane giving a lineation; interpreted to indicate that the lineation trend is most likely a flow feature (Figure 11a); (2) good clustering of χ_3 near the vertical with girdles of χ_1 and χ_2 giving a foliation but no lineation; samples in this category do not yield a flow direction (Figure 11b); (3) random orientations of χ_1, χ_2, and χ_3; interpreted to be the result of low degrees of anisotropy, or a result of turbulent emplacement (Figure 11c); and (4) good clustering of χ_1 and χ_2 while χ_3 is inclined at some angle ($<30^\circ$) from the vertical; interpreted to represent an imbrication (and hence indicating the apparent flow direction) or caused by postemplacement tilting (Figure 11d).

Examples of AMS plots "category 1" are exemplified by sample sites T36, T38, and T48. Site T36 is from the base of the OTT and has a foliation and azimuth plunging 13° at S55°W. The foliation dip is interpreted to represent imbrication and is usually well developed near the base of the flow unit. Therefore, the magnetic fabric at this site suggests that the source was to the southwest with flow to the northeast (Figure 12a). The data for site T38 are from incipiently welded, normally magnetized YTT and show a very tight cluster, indicating a good lineation and imbrication direction trending N41°E and plunging 12°SW. The lineation and imbrication directions also indicate a source to the SW (Figure 12c). Samples from locality T48 are interpreted as outflow deposits of welded YTT in which the AMS lineation and

TABLE 3. Anisotropy of Magnetic Susceptibility Data Determined From Welded Ignimbrites From Lake Toba, North Sumatra

			$\bar{X}_1$		$\bar{X}_2$		$\bar{X}_3$							
Locality	N_1/N_2	$\bar{X}\times10^{-3}$	D_{max}	I_{max}	D_{int}	I_{int}	D_{min}	I_{min}	$\bar{H}$	$\bar{V}$	l	f	X_1/X_2	X_2/X_3
T-1	6/4	2.0701	79.5	-5.1	349.7	4.6	120.4	82.9	4.5	48.4	0.020	0.025	1.020	1.026
T-2	6/4	2.0000	55.3	-7.7	325.2	-0.6	52.6	82.3	3.6	62.1	0.011	0.028	1.009	1.029
T-3	6/4	2.1309	116.0	-14.5	25.5	-1.9	108.8	74.9	4.3	64.1	0.008	0.035	1.008	1.036
T-4	6/6	6.4412	192.5	50.6	85.2	16.5	352.5	34.8	2.5	39.9	0.012	0.012	1.013	1.012
T-5	6/6	1.6896	179.9	-19.2	90.1	-11.7	211.5	47.7	4.4	45.7	0.020	0.024	1.020	1.024
T-6	6/3	0.8782	6.6	29.5	93.8	-1.7	185.6	57.5	9.7	43.5	0.021	0.015	1.021	1.015
T-8	6/4	2.5704	330.9	28.5	49.1	-18.6	112.8	57.9	3.5	62.9	0.008	0.028	1.007	1.028
T-9	6/4	48.7779	349.4	1.4	80.2	16.6	252.7	76.5	2.9	52.0	0.001	0.001	1.001	1.001
T-11	6/4	0.7216	351.0	6.3	81.2	-2.5	169.9	88.6	8.0	56.8	0.024	0.059	1.023	1.061
T-12	6/3	2.2067	329.0	-3.9	58.8	2.9	300.4	84.1	5.1	42.9	0.028	0.023	1.028	1.024
T-13	6/6	2.2721	127.1	15.0	38.1	-4.1	322.7	74.7	6.3	48.5	0.027	0.036	1.027	1.038
T-14	6/6	1.6413	121.3	6.5	31.9	21.0	235.0	72.5	3.1	63.3	0.007	0.025	1.007	1.026
T-18	6/6	2.9653	353.5	1.4	83.6	-3.8	94.2	83.4	3.0	52.9	0.010	0.021	1.010	1.021
T-19	6/5	4.2243	4.2	-7.8	94.5	-2.0	37.3	81.8	2.5	45.0	0.013	0.012	1.013	1.013
T-20	4/4	4.3677	133.4	-0.8	41.6	-9.5	8.7	73.3	2.4	47.6	0.011	0.012	1.011	1.013
T-21	4/4	5.5980	72.4	3.2	340.3	-0.5	195.0	87.6	1.5	57.2	0.005	0.010	1.005	1.010
T-22	6/6	2.0782	45.6	-5.3	135.8	10.1	7.6	77.4	4.8	57.0	0.014	0.033	1.014	1.034
T-23	6/4	6.8486	61.0	21.1	325.2	15.3	201.8	63.3	2.8	49.1	0.013	0.016	1.013	1.016
T-24	6/5	4.4826	83.7	-4.4	357.5	11.4	169.3	78.5	2.9	62.3	0.006	0.023	1.006	1.023
T-25	6/4	4.4475	123.8	-0.8	30.7	3.3	254.1	86.4	2.8	54.2	0.010	0.017	1.010	1.017
T-26	5/5	6.2469	337.3	8.2	71.6	24.5	230.0	63.9	2.9	56.0	0.010	0.020	1.010	1.020
T-27	3/3	2.7587	349.9	-2.9	78.1	34.1	264.5	53.4	2.2	64.4	0.004	0.017	1.004	1.017
T-29	6/6	2.3190	320.9	-10.6	55.0	1.9	336.3	80.2	6.1	51.6	0.024	0.038	1.024	1.039
T-30	6/5	1.4053	22.3	2.4	112.7	4.1	247.0	86.2	4.7	57.6	0.013	0.035	1.013	1.036
T-31	6/6	3.4951	23.6	11.1	114.6	2.2	217.8	80.2	4.1	65.3	0.007	0.036	1.007	1.037
T-32	6/6	3.3101	354.3	-10.8	76.4	24.7	292.5	64.2	3.2	39.0	0.019	0.013	1.019	1.013
T-33	6/6	4.5728	349.1	14.5	112.2	65.4	72.2	-19.3	3.1	45.1	0.016	0.015	1.016	1.015
T-36	6/5	1.5834	54.7	-13.1	326.7	9.7	89.6	74.0	8.1	53.4	0.027	0.049	1.027	1.050
T-37	6/5	1.3153	354.0	-12.9	84.1	7.8	321.6	71.8	4.5	54.1	0.015	0.030	1.015	1.031
T-38	6/6	1.4992	41.2	-11.8	132.4	-5.1	61.3	76.5	8.8	59.8	0.023	0.067	1.022	1.071
T-39	6/6	1.0247	6.4	-25.2	95.7	-3.0	9.0	63.4	3.8	47.8	0.017	0.021	1.017	1.022
T-40	6/6	2.2065	33.0	-7.7	316.3	50.5	122.0	40.4	3.5	46.3	0.008	0.009	1.008	1.009
T-41	6/6	1.1646	99.1	56.0	108.8	-26.0	16.2	-6.1	3.6	58.3	0.009	0.027	1.009	1.027
T-42	6/6	1.5409	56.0	49.3	112.2	-21.7	11.2	-33.5	3.6	47.8	0.019	0.018	1.019	1.019
T-43	6/6	1.1634	26.3	19.3	109.8	-12.6	171.3	63.0	3.8	48.2	0.016	0.024	1.016	1.025
T-44	6/6	1.5425	79.2	20.5	98.8	74.8	226.4	43.0	2.7	42.8	0.016	0.012	1.016	1.012
T-45	6/5	1.2100	319.9	3.4	49.4	4.5	188.8	83.3	5.1	56.4	0.015	0.034	1.015	1.035
T-46	6/6	0.9968	330.4	54.9	47.7	-8.8	128.5	45.8	3.4	44.7	0.017	0.017	1.017	1.017
T-47	6/6	1.7791	15.3	7.3	97.6	-8.6	67.4	86.2	4.7	50.6	0.019	0.028	1.025	1.028
T-48	6/4	1.3801	78.7	-10.4	347.6	-6.8	45.5	77.7	5.1	47.9	0.022	0.035	1.022	1.036
T-49	6/5	1.2469	50.6	30.0	324.8	-6.9	243.5	60.8	6.2	49.8	0.029	0.031	1.029	1.032
T-50	6/5	1.5252	5.3	14.8	100.0	11.7	227.0	69.7	4.3	58.2	0.012	0.031	1.012	1.031
T-51	6/6	1.4511	325.8	-1.4	31.7	11.6	277.9	85.5	5.4	46.7	0.025	0.027	1.025	1.028
T-52	6/4	3.3057	29.5	-15.6	297.8	-14.6	339.6	67.3	3.3	37.0	0.012	0.022	1.012	1.022
T-53	6/4	0.7195	70.9	2.2	352.0	41.8	343.4	47.7	2.6	44.6	0.012	0.016	1.012	1.016

T-54	6/6	3.3801	84.3	23.8	357.6	-2.1	277.9	69.0	6.3	58.5	0.018	0.044	1.018	1.046
T-55	6/4	0.9542	95.0	-21.7	359.5	-10.9	69.1	64.3	9.7	48.5	0.029	0.068	1.039	1.055
T-56	6/6	2.5797	13.4	7.6	111.9	-16.7	115.4	73.0	4.4	48.8	0.018	0.026	1.018	1.026
T-57	6/5	0.6016	52.1	19.8	323.5	-1.4	229.0	66.1	7.3	46.3	0.033	0.040	1.033	1.042
T-58	6/6	29.4509	329.5	-18.3	65.2	-24.2	13.9	61.4	6.2	57.6	0.001	0.003	1.001	1.003
T-60	6/6	1.7169	99.0	-21.7	359.2	-16.1	59.5	64.1	8.4	54.3	0.030	0.054	1.030	1.056
T-61	6/6	4.2971	67.1	-29.2	340.4	8.6	80.2	64.1	5.0	47.4	0.015	0.016	1.015	1.016
T-62	6/6	1.4976	344.4	20.5	76.7	11.8	232.8	71.0	2.6	47.5	0.011	0.014	1.011	1.014
T-63	6/4	5.1723	63.6	1.0	333.8	-10.5	331.3	77.9	4.2	55.5	0.013	0.028	1.013	1.029
T-64	6/5	8.9985	132.8	10.5	39.6	16.3	253.4	69.8	3.4	59.2	0.008	0.019	1.008	1.019
T-65	6/6	3.3694	331.3	6.6	66.5	35.0	225.5	54.7	4.5	68.9	0.006	0.039	1.006	1.040
T-66	6/6	305.6961	346.4	10.3	79.9	20.7	229.5	65.4	1.0	59.3	0.000	0.001	1.000	1.001
T-67	6/4	1.6228	28.6	19.1	120.8	6.3	228.6	71.7	7.7	60.7	0.011	0.041	1.011	1.043
T-68	6/5	5.3502	91.6	-9.8	1.2	-10.2	47.3	77.0	4.6	53.4	0.012	0.023	1.012	1.023
T-69	6/6	7.9086	346.7	-4.2	75.9	9.9	283.4	79.6	2.4	55.8	0.009	0.014	1.009	1.014
T-70	6/4	5.2500	9.4	4.5	100.0	1.4	240.3	84.3	3.3	51.7	0.013	0.018	1.013	1.018
T-71	6/6	0.6810	108.0	-14.8	21.7	21.8	151.2	69.2	4.8	40.7	0.033	0.023	1.033	1.024
T-72	6/4	8.0205	28.3	29.3	121.0	-0.3	204.9	64.9	1.7	37.0	0.012	0.006	1.012	1.006
T-73	6/5	5.8419	11.4	10.0	104.1	2.2	204.3	78.8	1.8	49.7	0.008	0.010	1.008	1.011
T-74	6/4	1.2007	33.7	7.6	124.3	1.7	219.8	82.8	8.8	55.2	0.032	0.057	1.032	1.060
T-75	6/4	1.6687	349.2	3.2	87.8	-21.3	80.7	65.3	8.6	46.8	0.047	0.043	1.047	1.045
T-76	6/4	3.6021	316.6	22.3	72.7	43.0	30.2	-38.0	4.2	57.2	0.014	0.026	1.014	1.027
T-77	6/4	1.2287	355.3	-1.1	87.1	10.8	252.2	80.0	4.8	44.5	0.022	0.026	1.022	1.027
T-78	6/6	1.5983	113.7	25.1	19.5	33.9	216.3	51.8	5.4	42.3	0.031	0.023	1.031	1.023
T-79	6/6	2.1685	23.4	12.6	107.5	33.9	229.6	63.0	5.1	56.5	0.018	0.033	1.018	1.033
T-80	6/4	4.8133	12.7	19.9	109.3	17.7	237.9	64.0	3.2	56.8	0.011	0.021	1.011	1.021
T-83	6/5	1.7956	323.5	4.3	58.2	15.1	44.2	-72.5	4.1	41.4	0.018	0.022	1.018	1.022
T-84	6/6	3.9780	315.2	-3.6	358.5	-16.9	51.8	-24.0	3.4	30.0	0.010	0.024	1.001	1.025
T-85	6/6	1.4438	258.1	-8.5	166.0	-7.5	40.8	-79.2	6.6	43.8	0.032	0.033	1.032	1.034
T-86	6/6	0.8856	349.0	0.4	58.7	26.2	268.0	52.8	7.8	43.9	0.042	0.030	1.042	1.031
T-87	6/6	2.5752	107.3	16.8	14.9	26.4	232.4	64.6	7.6	51.0	0.031	0.045	1.031	1.047
T-88	5/4	1.8134	31.6	35.4	339.1	39.4	281.2	28.6	3.9	47.7	0.017	0.018	1.017	1.019
T-89	6/6	1.4913	4.4	9.6	271.0	10.5	281.7	-74.8	5.2	41.1	0.022	0.031	1.022	1.032
T-91	6/5	1.0868	37.4	-14.4	130.2	-17.8	90.0	65.0	8.1	51.2	0.039	0.049	1.038	1.052
T-92	6/6	1.6937	59.8	3.1	328.9	14.5	154.7	77.1	9.1	46.0	0.041	0.050	1.041	1.053
T-93	6/6	2.7104	277.8	12.1	3.1	22.4	31.7	64.8	2.8	30.5	0.007	0.021	1.007	1.022
T-94	5/5	5.9052	113.1	13.8	19.9	11.7	252.0	71.9	3.9	62.8	0.008	0.030	1.008	1.031
T-96	6/5	4.4642	89.9	-10.7	357.8	16.1	34.2	-69.4	1.7	38.6	0.006	0.010	1.006	1.010
T-97	6/4	1.9002	22.2	-15.9	294.8	9.3	54.5	-71.5	7.0	49.3	0.037	0.027	1.037	1.028
T-98	6/6	1.6915	16.8	48.4	312.1	13.2	35.0	38.2	3.5	42.9	0.016	0.019	1.017	1.020
T-99	6/4	1.4540	1.0	23.8	88.8	4.6	347.1	64.3	3.3	28.4	0.007	0.024	1.007	1.025
T-100	6/5	2.9467	293.8	8.1	25.7	11.1	359.0	85.0	3.2	39.4	0.014	0.019	1.014	1.019

Mean AMS data for samples collected in 1984 and 1985 and measured at UTA and UH: N_1/N_2 is the total number of samples per site over the number of samples used in the final AMS mean results (e.g., N_1/N_2=6/6 indicates that no samples were rejected from the mean calculations); X_1, X_2, and X_3 are the mean susceptibility directions as described in the text; H is the mean total anisotropy at each site; V is the mean Graham's value at each site; "l" and "f" are the quantitative measures of the lineation and foliation respectively as defined in the text; X_1/X_2 and X_2/X_3 are the axial magnitude ratios.

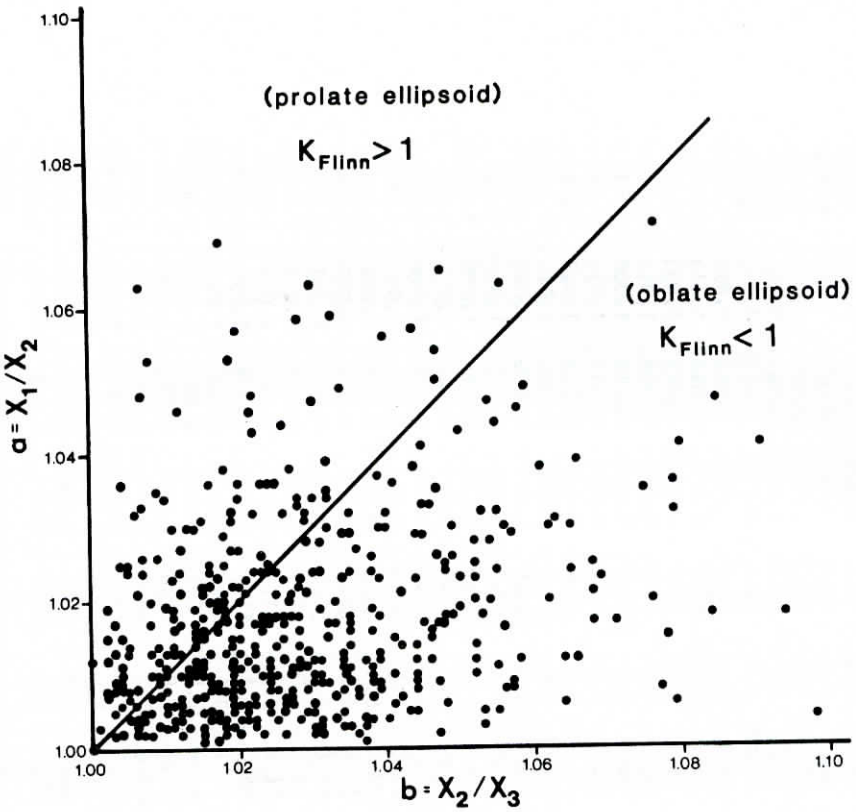

Fig. 10. Two-axis plot "Flinn diagram" of χ_2/χ_3 versus χ_1/χ_2 for 538 samples (see text for explanation). Twenty-five percent of the samples are dominated by magnetic grains that have an elongated (prolate) shape, while a majority of the ignimbrites contain magnetic grains that have flattened (oblate) tendencies similar to the results shown in Figure 9. K_{Flinn} as defined by Flinn [1962].

imbrication directions plunge 10° at S79°W. The AMS data indicate a source to the W or SW in the northern portion of Lake Toba in agreement with the grain size distribution pattern of Caress [1985]. Sites T38 and T48 suggest two separate source regions at opposite ends of the lake for the YTT.

Examples of "category 2" AMS plots, which indicate the foliation direction, are represented by sites T4, T18, and T24. Site T4 sampled an andesitic rheoignimbrite that predates the Toba tuff eruptions. Because AMS orientation for this site is quite interesting and somewhat atypical of the welded ignimbrites found around Lake Toba, it is discussed here.

Rheomorphism of welded tuff is related to secondary mass flow that occurred shortly after emplacement while the ignimbrite was still a hot coherent viscous fluid [Wolff and Wright, 1981]. Compaction and welding of tuff is a simple flattening process and results in the classic eutaxitic texture [Ragan and Sheridan, 1972] in which the resulting strain ellipsoid is oblate with K∿0 [Flinn, 1962; Ramsay, 1967]. The resulting magnetic fabric in such tuffs should therefore be initially oblate and horizontal due to compaction. Rheomorphism imposes a secondary stretching deformation, resulting in a tendency toward the development of a prolate fabric, and a parataxitic texture which can easily be observed in the field by the presence of elongated fiamme having a spindle-shaped form. Lithic clasts may be rotated and have void spaces or hollow pockets at each end [Schmincke and Swanson, 1967]. These features characterize the rheoignimbrite T4 at Haranggaol. The AMS data define a foliation plane dipping at 55°. Secondary flowage is supported by the mean Graham's V value of 40° (e.g., V is 45° or greater for undisturbed sediments; Table 3). Alternatively, posttectonic tilting may have rotated this whole block, resulting in the direction anomalies.

At site T18 (eastern side of Samosir Island), χ_1 and χ_2 define a foliation plane striking N4°E and of shallow dip (7° NW, Figure 12b). This moderately welded ignimbrite is MTT that possibly represents the uppermost portion of caldera filling. The AMS data for site T24 define a foliation plane dipping 12° toward N11°W (Figure 12a). The present attitude of the magnetic fabric could define the imbrication direction; however, there is also evidence for some degree of postemplacement tectonic tilting based on the NRM direction for this site (D = 190.2, I= -11.2). Possibly the true dip is more like 1°, and if so there is no evidence for imbrication.

Examples of "category 3" type AMS plots are represented by sites T5, T20, and T21. The mean principal axes show much scatter, suggesting that deposition occurred under near-source turbulent flow conditions. Site T5 in the Prapat graben is massive, incipiently welded YTT, and its coarse-

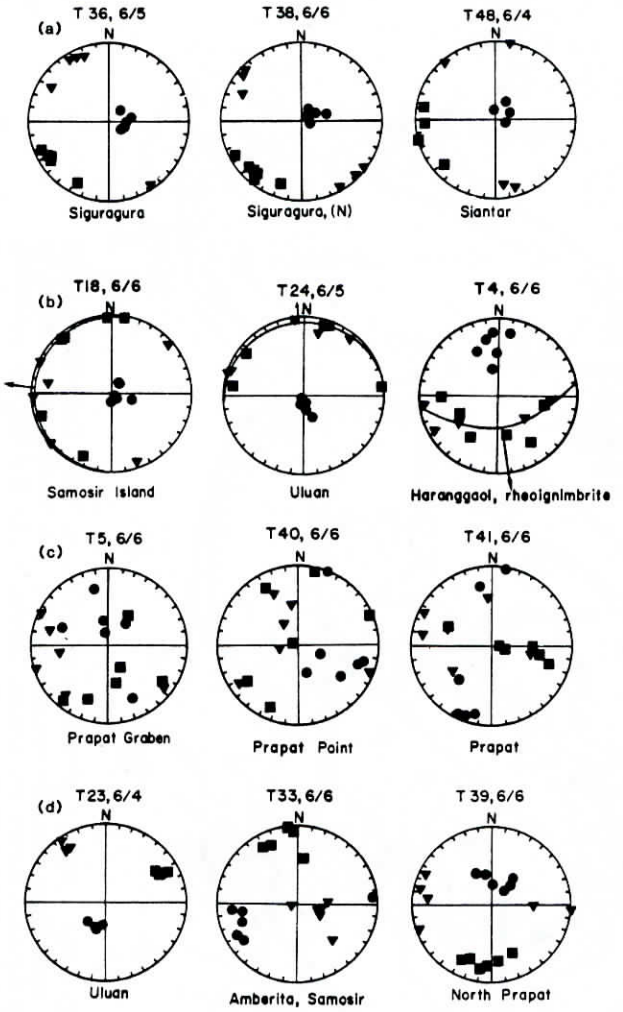

Fig. 11. AMS equal-area lower hemisphere plots of χ_1 (solid squares), χ_2 (solid triangles) and χ_3 (solid circles). (a) Category 1 AMS plots. (b) Category 2 AMS plots. (c) Category 3 AMS plots. (d) Category 4 AMS plots. See text for explanation.

grained nature (average maximum lithic size is 12.5 cm) suggests that this locality is near a source vent. At sites T20 and T21 on the southeast shore of Samosir, only four samples of densely welded MTT were collected at each site, and both show much scatter and an anomalous bimodal distribution in χ_1, with two lineation directions at nearly 90°. The scatter in the AMS data and the general lack of any imbrication indicate a change in flow regime from turbulent at sites T20 and T21 to laminar farther north as was suggested elsewhere by Mimura and MacLeod [1978] and Kamata and Mimura [1983].

Summary diagrams of all the AMS data measured at UTA are shown in Figures 12a-12c and indicate the possible flow direction(s) of the Lake Toba ignimbrite(s) based on the mean χ_1 AMS lineation direction (small arrows) at localities that show a well-grouped distribution of χ_1 susceptibility directions, with or without an imbrication direction. The cone of confidence for the mean lineation directions ranges from 10° to 30°. Based on the AMS data both the OTT and MTT are inferred to have been erupted from multiple vents aligned along a fissure extending NW-SE for several tens of kilometers (stars shown in Figures 12a and 12b). The YTT was erupted mainly from two separate vents some 65 km apart in the north and south ends of the lake (Figure 12c).

Microsocopic Flow Orientation Studies

The microscopic techniques used to determine the flow direction of ash flows were developed by Elston and Smith [1970] and Rhodes and Smith [1972]. These techniques were applied to 20 samples from Lake Toba to provide a direct comparison with AMS data by cutting thin sections parallel to the foliation from the same cores used for the AMS study. The preferred orientation of elongated crystals, pumice, and lithic clasts in such oriented thin sections describe a flow lineation resulting from primary flow [Elston and Smith, 1970]. The thin sections were projected on paper, and the long axes of crystals or clasts for which the length:width ratio exceeded 2:1 were plotted. Between 100 and 200 grains were measured for each section. The trend of the long axis of each grain relative to north was measured, and the number of grains having their long axis lying in each 10° sector was counted and plotted on rose diagrams (Figure 13). A preferred orientation was observed in all but one of the oriented samples. Nine of the thin sections cut parallel to the foliation agree to within 30° of the measured χ_1 (AMS) lineation trend, and four agree to within ±10° (Figure 13). The presence of a magnetic-fabric imbrication with a low-angle dip of less than 10°-30° to the foliation plane defines the flow direction of the ignimbrite. A small pilot group of four samples was chosen to determine if an imbrication was visible in oriented thin sections cut perpendicular to the foliation, and three showed a distinct imbrication that agreed with the imbrication inferred from the AMS measurements. The statistical significance of the flow lineation data was analyzed using the chi-square test [Tukey, 1954], which showed that the data distribution is nonrandom at the 95% confidence level.

Eruptive History of the Toba Caldera

Using the reversal sequence, AMS and microscopic flow orientation determination, and grain size characteristics, a geologic history for Lake Toba can be developed. The Toba depression is associated with thick accumulations of densely welded, incipiently welded, and nonwelded rhyolitic ignimbrites produced by tremendous episodic explosive eruptions. Caldera subsidence accompanied each eruption, and where the ignimbrites are thickest within the Toba depression they are of intracaldera type [cf. Ross and Smith, 1961; Smith, 1979]. Rise of new magma to reinflate the magma chamber caused resurgent updoming of the caldera floor with development of longitudinal grabens on the domes. Trapdoor uplift also may have occurred.

First Eruptive Phase

Large andesitic volcanoes, remnants of which can be seen in the north and south walls of the Toba depression, were already present when the

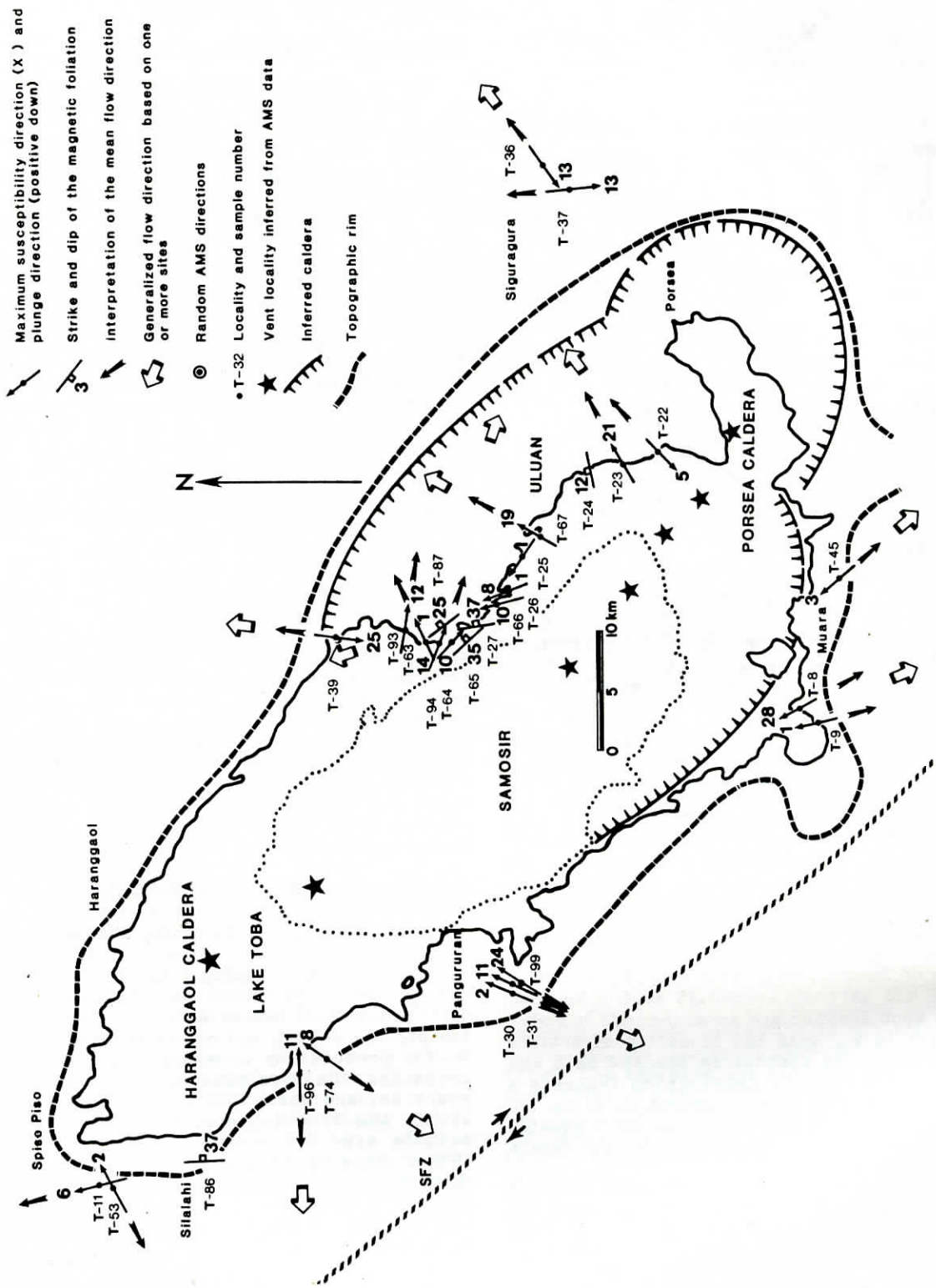

Fig. 12a. Summary diagram of AMS data for the oldest ignimbrite eruption (OTT) at Lake Toba. Flow directions are derived from the mean X_1 AMS lineation directions for each site and represented by large solid arrows. The inferred vent localities (stars) are shown schematically and may be isolated, active points aligned along a NW-SE trending fissure system.

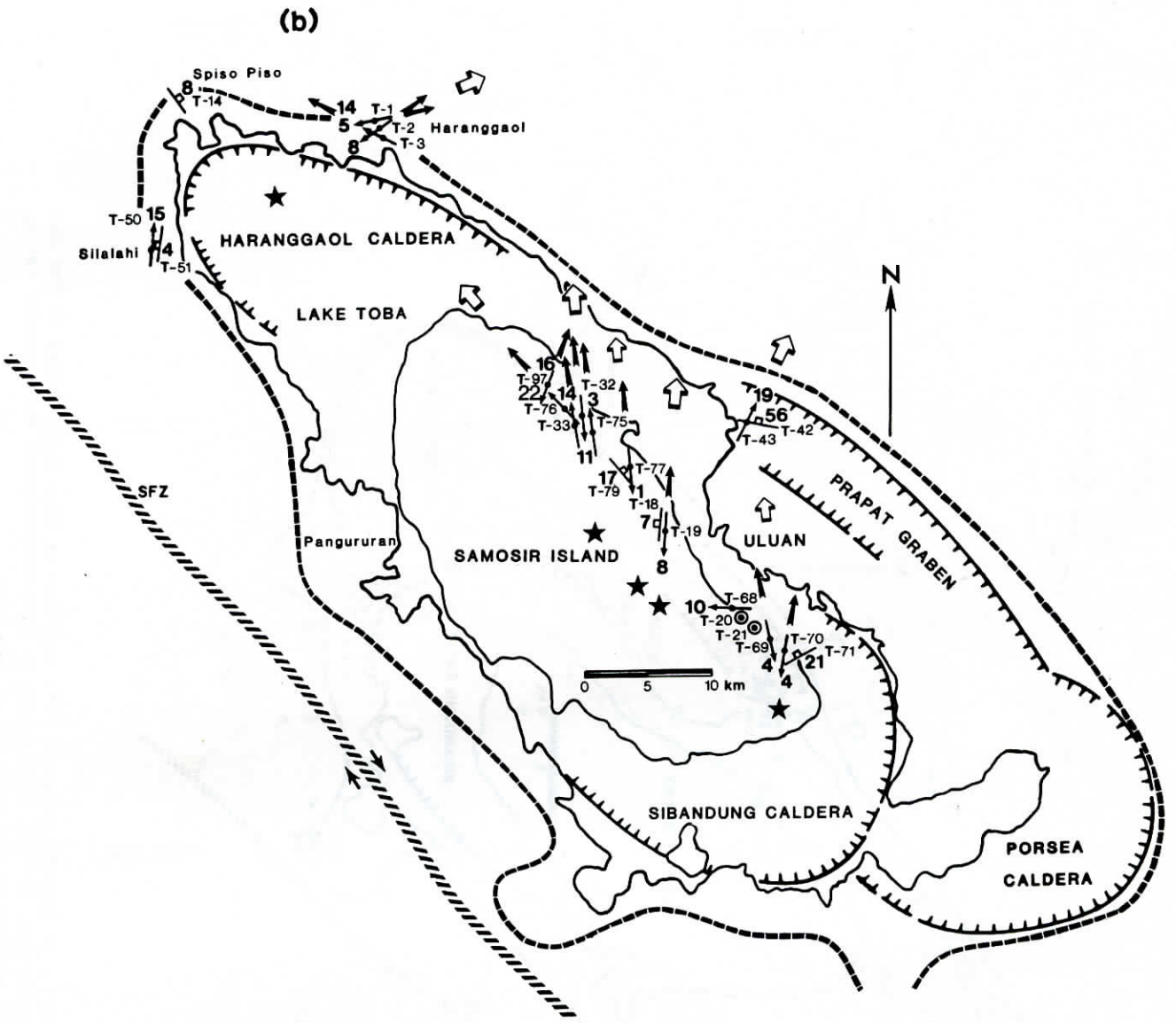

Fig. 12b. Summary diagram of AMS data for the intermediate (MTT) eruption at Lake Toba. The inferred vents occurred in two separate calderas (i.e., Haranggaol and Sibandung calderas). Vents in the Sibandung caldera may have been aligned along a fissure system very similar to that of the OTT and could be explained as a NW propagation of the OTT fissure system.

first eruption occurred. Associated with these older volcanoes in the north is a reversely magnetized andesitic rheoignimbrite (> 200 m thick) that covered more than 700 km^2 at the north end of the depression.

At about 0.84 Ma the OTT ignimbrite was erupted from a fissure source in the southern portion of the Toba depression and a second source in the north (Figure 14a). The OTT is thickest at Uluan and apparently infills the Porsea caldera and its extension to the NW in Uluan. The western and northern limits of the caldera are not known. The maximum lithic size does not vary much but reaches a maximum of 8.2 cm at Uluan. The AMS lineation and flow direction data do not point to a single source but indicate that it erupted from a fissure vent extending several tens of kilometers and oriented NW-SE parallel to the Sumatran Fault Zone. It is possible that the next stage was major resurgence, where more than 500 m of uplift of the caldera floor occurred to generate the NW-SE-trending elongated dome of Uluan (Figure 14b). Only a part of this dome has survived.

Second Eruptive Phase

The MTT ignimbrite appears to have originated from two separate sources, a main one in Samosir and a second one located at the far north end within the Haranggaol caldera (Figure 14c). The main MTT outcrop along the east side of Samosir is more than 300 m thick and is thought to be a caldera infill (Sibandung caldera, Figures 14c and 14f). AMS data indicate a fissure source extending about 20 km in a NW-SE direction, similar to that for the OTT, which is now concealed beneath

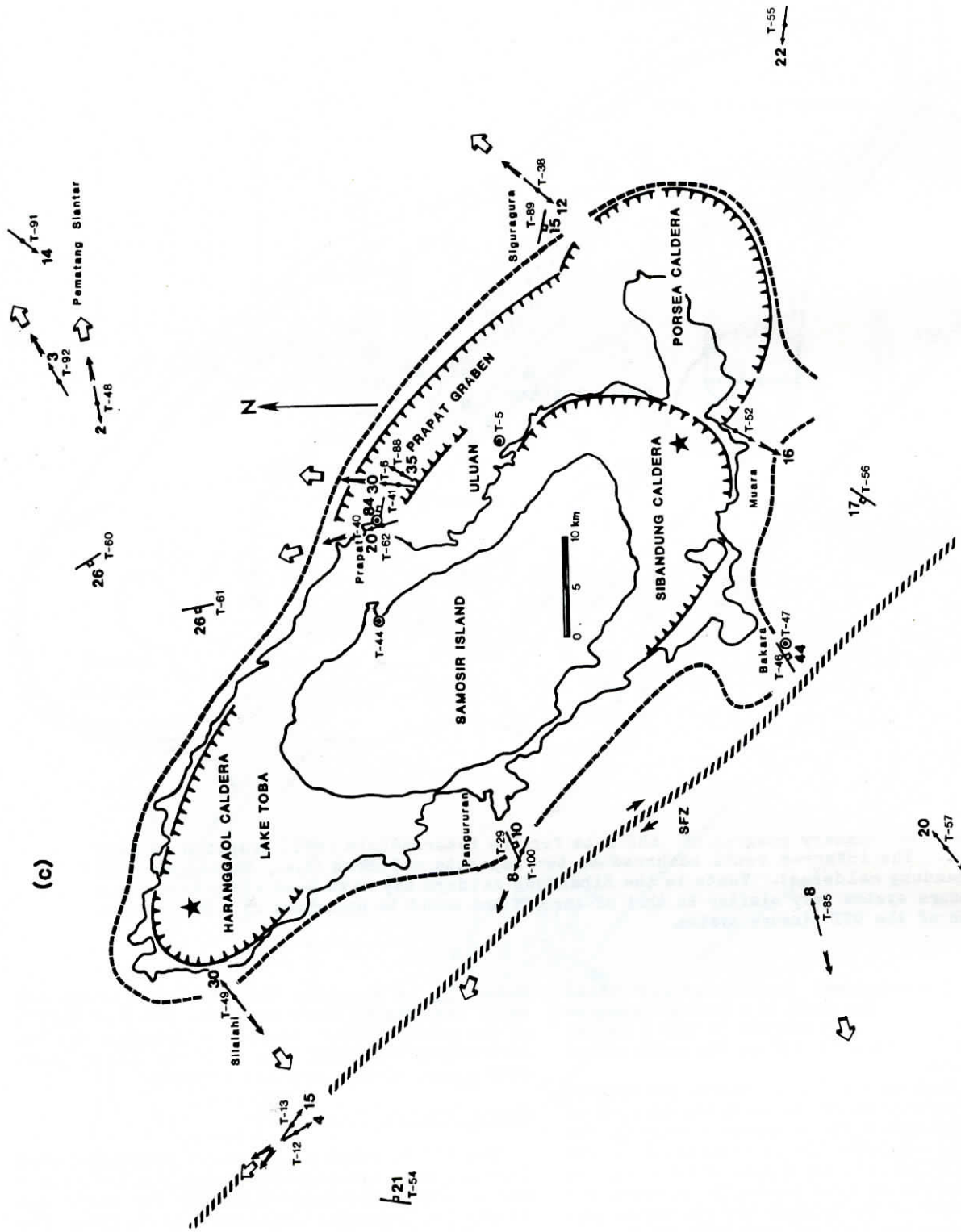

Fig. 12c. Summary diagram of AMS data for the youngest (YTT) eruption at Lake Toba. Based on the AMS data (mainly within the outflow sheets), the YTT is inferred to have erupted from two separate vents, one located in the far north and another at the south end of the lake.

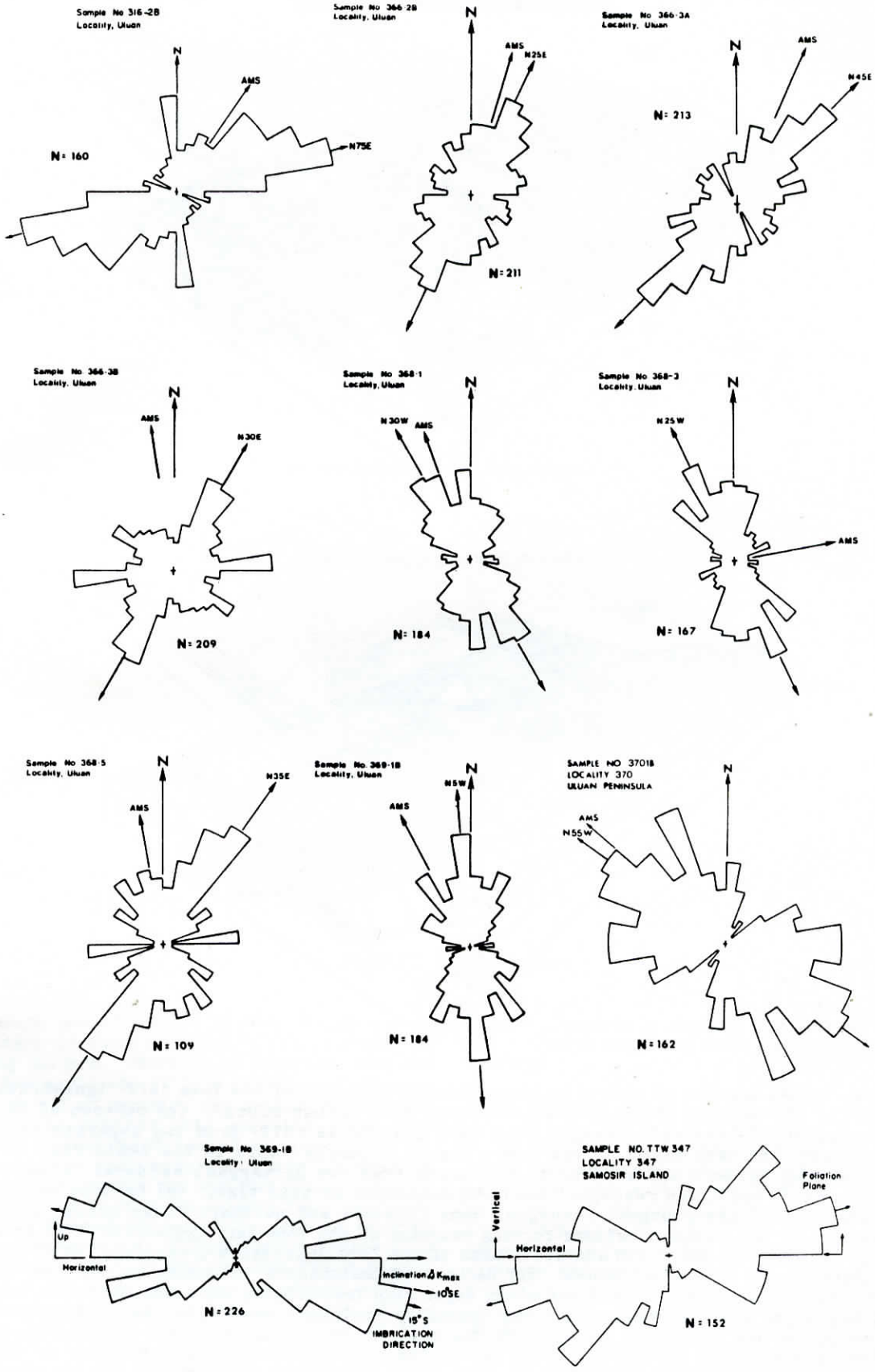

Fig. 13. Rose diagrams of mean lineation direction or foliation direction (arrowhead) calculated from oriented thin sections. Note that the AMS directions for each sample are also shown.

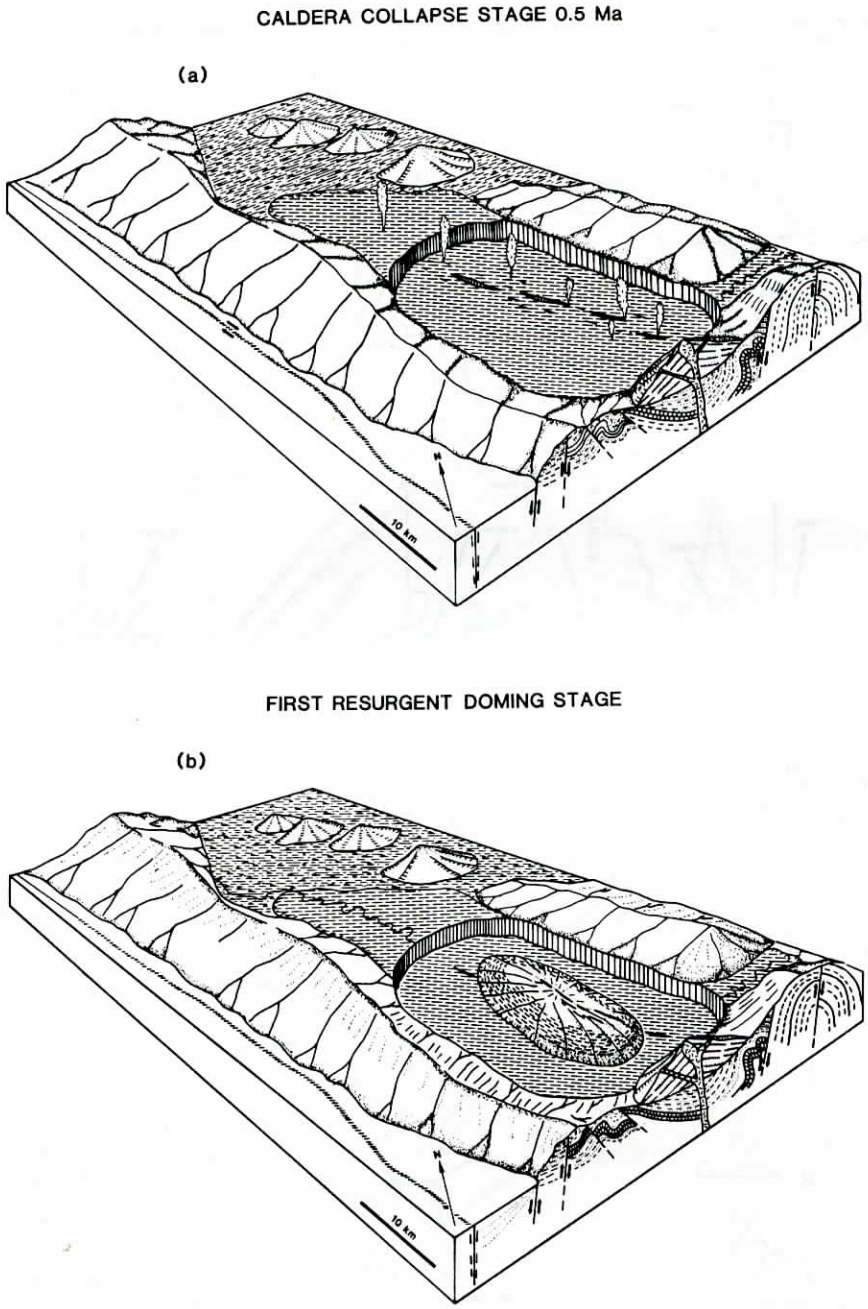

Fig. 14. (a) Cartoon of oldest caldera-forming eruption of the Toba tuff ignimbrite (OTT). (b) Cartoon of the oldest resurgent dome (Uluan Block). (c) Cartoon of the formation of intermediate-aged Toba tuff ignimbrite (MTT) from two separate vent sources; the main eruption was from aligned multiple vents in the south from the Sibandung caldera and another to the north from the Haranggaol caldera. A major portion of the Uluan resurgent dome was destroyed at this time. (d) Cartoon of the formation of the youngest resurgent dome (Samosir and northern Uluan blocks). (e) Cartoon of the youngest caldera-forming eruption of the Toba tuff ignimbrite (YTT) from two calderas at the north and south ends of the Toba depression (reactivation of the Sibandung and Porsea calderas). (f) Cartoon of postcaldera volcanism in the form of rhyolitic to andesite lava domes along major ring fractures in the south and north, and along major linear-graben structures (possibly contemporaneous with the formation of the Latung and Pangururan grabens). On the map, (1) represents the first eruptive phase (formation of the Porsea caldera), (2) the second eruptive phase (formation of the Haranggaol and Sibandung calderas in the north and south respectively), (3) the third and largest eruptive phase (reactivation of Haranggaol, Sibandung, and Porsea calderas from vents in the northern and southern parts of the lake), (4) the Uluan Block, (5) the Samosir Block, and (6) the Sumatran Fault Zone.

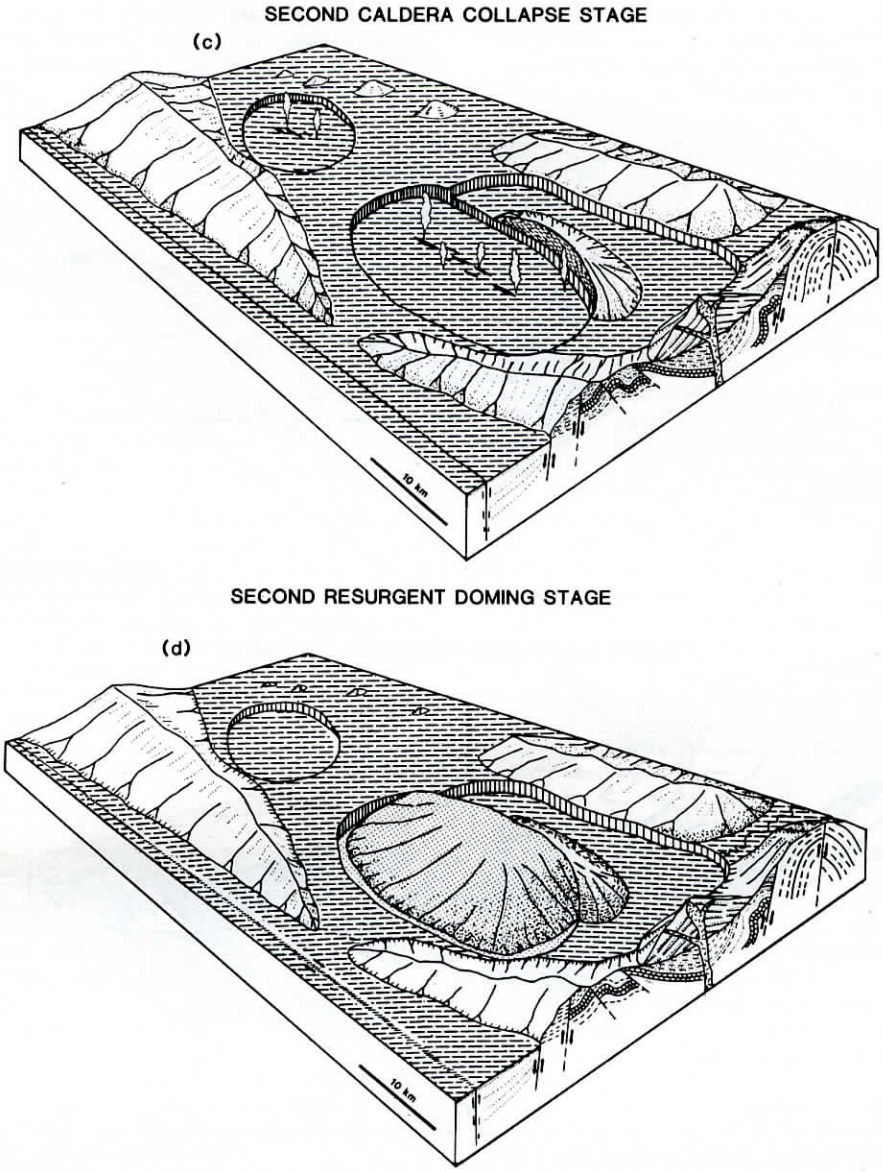

Fig. 14. (continued)

the southern end of Samosir Island. The extent of the caldera is uncertain but could embrace the Sibandung caldera. There is no certainty that the MTT at the north end of Lake Toba is of the same age as the MTT of Samosir, and reliable age dates are needed to resolve this question. The next event was a prolonged period of deposition of coarse clastic sediments and later lacustrine sediments over Samosir and northern Uluan. Uplift then took place to form the asymmetrical half-dome of Samosir Island (Figure 14d). It is thought that the northern part of Uluan was uplifted also at this time. Whether the Samosir/Uluan massif represents two separate updoming stages, as presented here, or a single dome which has subsequently been asymmetrically rifted along the Latung graben may never fully be resolved. However, based on the presence of coarse breccias directly overlying the ignimbrite deposits of SE Samosir and the lack of similar such deposits found along southern Uluan a single updoming stage cannot adequately explain the present stratigraphy. Therefore, two dome building stages are inferred.

Third Eruptive Stage

At about 0.075 Ma the largest of the three major ignimbrite-forming eruptions occurred at Lake Toba. As much as 2000 km^3 of YTT ash flow and 2000 km^3 of ashfall were erupted, and the former traveled as far as 100 km from its source. Eruption was from major vents 65 km apart in the northern and southern parts of the lake where the two calderas of Haranggaol and Sibandung formed synchronously (Figure 14e). The Prapat graben and Porsea caldera were filled with YTT, and renewed subsidence occurred of the Porsea caldera [Caress, 1985]. The Latung graben may have also developed along a fissure joining the two main YTT vents. The final volcanic stage saw the formation of several rhyolitic and andesitic lava domes along

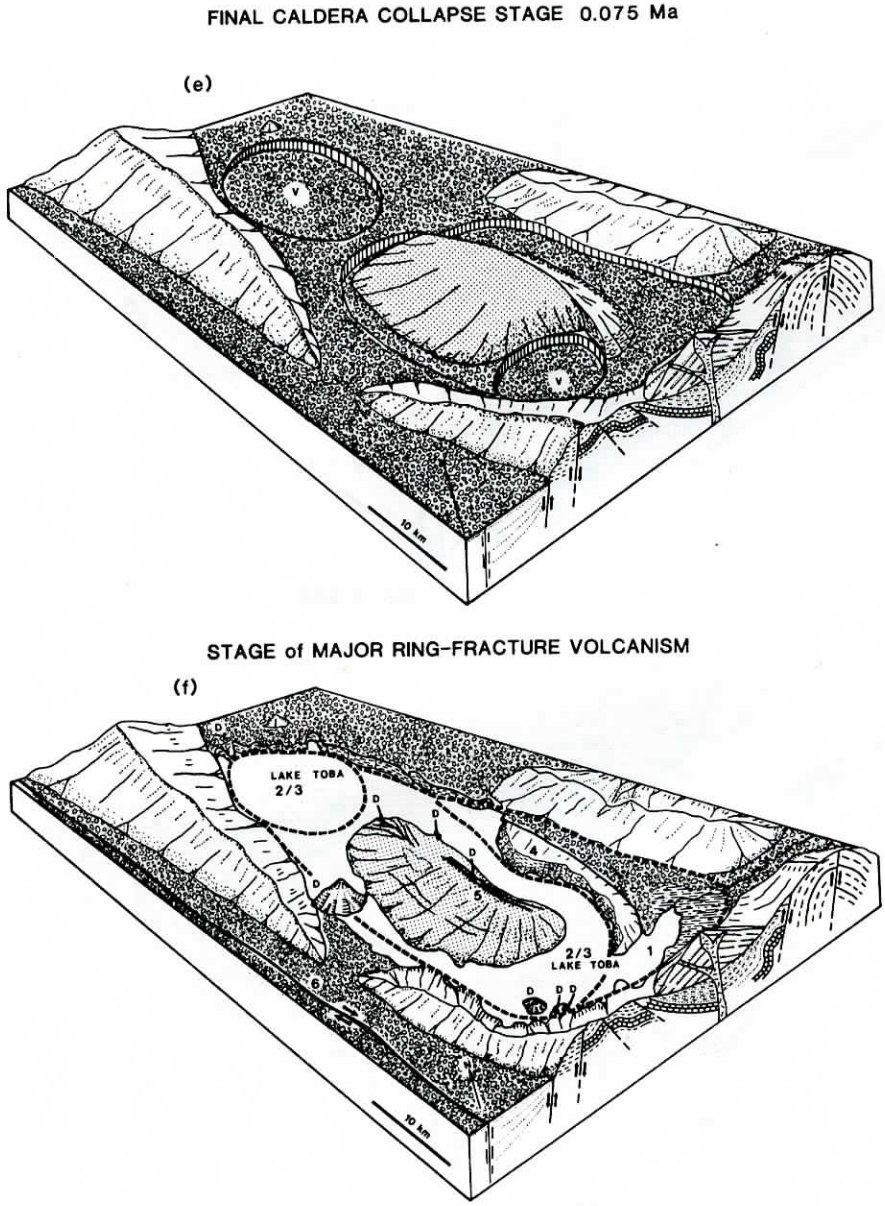

Fig. 14. (continued)

preexisting lines of weakness, namely graben faults, and at Muara along a ring fault (Figure 14f).

Acknowledgments. This project was supported under National Science Foundation grant EAR 82-06655. We are grateful for the cooperation with the Volcanological Directorate of Indonesia in Bandung, Java, and Peter E. Hehanussa of the Indonesian Institute of Sciences (L.I.P.I.). Special thanks is also expressed to Robert S. Coe for the use of the low-field torque magnetometer at the University of California at Santa Cruz and to William I. Rose, Jr., for his comments while in the field and during the editing of this manuscript. Hawaii Institute of Geophysics contribution 1767.

References

Aldiss, D. T., and S. A. Ghazali, The regional geology and evolution of the Toba volcano-tectonic depression, Indonesia, J. Geol. Soc. London, 141, 487-500, 1984.

Aramaki, S., Formation of the Aira Caldera, Southern Kyushu, ~22,000 years ago, J. Geophys. Res., 89, 8485-8501, 1984.

Bacon, C. R., Eruptive history of Mount Mazama and Crater Lake Caldera, Cascade Range, U.S.A., J. Volcanol. Geotherm. Res., 18, 57-115, 1983.

Barberi, F., F. Innocenti, L. Lirer, R. Munno, T. Pescatore, and R. Santacroce, The Campanian Ignimbrite: A major prehistoric eruption in the Neopolitan area (Italy), Bull. Volcanol., 41-1, 11-31, 1978.

Caress, M. E., Volcanology of the youngest Toba Tuff, Sumatra, M.S. thesis, 150 pp., Univ. of Hawaii, Manoa, 1985.

Chapin, C. E., and G. R. Lowell, Primary and secondary flow structures in ash-flow tuffs of the Gribbles Run paleovalley, central Colorado, in Ash Flow Tuffs, edited by C. E. Chapin and W. E. Elston, Spec. Pap. Geol. Soc. Am., 180, 137-154, 1979.

Chesner, C. A., Ages of ignimbrites from Toba caldera, Sumatra: Lessons in dating Quarternary volcanic rocks (abstract), Eos Trans. AGU, 65, 1134-1135, 1984.

Chesner, C. A. and W. I. Rose, Geochemistry, mineralogy and physical constraints of the Toba Ignimbrite (abstract), Eos Trans. AGU, 64(45), 873, 1983.

Curtis, G. H., Importance of Novarupta during eruption of Mt. Katmai, Alaska, in 1912 (abstract), Geol. Soc. Am. Bull., 66, 1547, 1955.

Day, R. M., M. Fuller, and V. A. Schmidt, Hysteresis properties of titanomagnetites: Grain-size and compositional dependence, Phys. Earth Planet. Inter., 13, 260-267, 1977.

Diehl, J. F., C. A. Chesner, and M. D. Knight, Further evidence for the Emperor Event from Lake Toba, Northern Sumatra (abstract), Eos Trans. AGU, 65, 869, 1984.

Druitt, T. H., and R. S. J. Sparks, A proximal ignimbrite breccia facies on Santorini, Greece, J. Volcanol. Geotherm. Res., 13, 147-171, 1982.

Ellwood, B. B., Estimates of flow direction for calc-alkaline welded tuffs and paleomagnetic data reliability from anisotropy of magnetic susceptibility measurements: Central San Juan Mountains, southwest Colorado, Earth Planet. Sci. Lett., 59, 303-314, 1982.

Ellwood, B. B., Anisotropy of magnetic susceptibility: Empirical evaluation of instrumental precision, Geophys. Res. Lett., 11, 645-648, 1984.

Ellwood, B. B., and C. Abrams, Magnetization of the Austell gneiss, northwest Georgia Piedmont, J. Geophys. Res., 87, 3033-3043, 1982.

Elston, W. E., and E. I. Smith, Determination of flow direction of rhyolitic ash flow-tuff from fluidal textures, Geol. Soc. Am. Bull., 81, 3393-3406, 1970.

Fisher, R. A., Dispersion on a sphere, Proc. R. Soc. London, 217, 295-305, 1953.

Fitch, T. J., Plate convergence, transcurrent faults, and internal deformation adjacent to Southeast Asia and the Western Pacific, J. Geophys. Res., 77, 4432-4460, 1972.

Flinn, D., On folding during three-dimensional progressive deformation, Geol. Soc. (London) Quart. J., 118, 385-433, 1962.

Froggatt, P. C., C. J. N. Wilson, and G. P. L. Walker, Orientation of logs in the Taupo Ignimbrite as an indicator of flow direction and vent position, Geology, 9, 109-111, 1981.

Graham, J. W., Significance of magnetic anisotropy in Appalachian sedimentary rocks, in The Earth Beneath the Continents, Geoghys. Monogr. Ser., vol. 10, edited by J. A. Steinhart and T. J. Smith, pp. 627-648, AGU, Washington, D. C., 1966.

Graham, J. W., Preliminary account of a refined technique for magnetic susceptibility anisotropy measurement of rocks, in Methods in Paleomagnetism, edited by D. W. Collinson, K. M. Creer, and S. K. Runcorn, 409-424, Elsevier, Amsterdam, 1967.

Hamilton, W., Tectonics of the Indonesian region, U.S. Geol. Surv. Prof. Pap., 1078, 345 pp., 1979.

Hildreth, W., and G. A. Mahood, Ring-fracture eruption of the Bishop Tuff indicated by accidental lithic fragments (abstract), Eos Trans. AGU, 65, 1149, 1984.

Hirooka, K., Paleomagnetism of Sunda Arc--Preliminary report on the study of physical geology of Sunda Island Arc, edited by S. Sasajima, pp. 18-23, Kyoto Univ., 1978.

Hutchinson, C. S., Indonesia, in Andesites, edited by R. S. Thorp, pp. 207-224, John Wiley and Sons, New York, 1982.

Incoronato, A., F. T. Addison, D. H. Tarling, G. Nardi, and T. Pescatore, Magnetic fabric investigation of some pyroclastic deposits from the Phlegrean Fields, Southern Italy, Nature, 306, 461-463, 1983.

Kamata, H., and K. Mimura, Flow directions inferred from imbrication in the Handa pyroclastic flow deposit in Japan, Bull. Volcanol., 46(3), 277-282, 1983.

Khan, M. A., Anisotropy of magnetic susceptibility of some igneous and metamorphic rocks, J. Geophys. Res., 67, 2873-2885, 1962.

King, R. F., and A. L. Rees, The measurement of the anisotropy of magnetic susceptibility of rocks, by the torque method, J. Geophys. Res., 67, 1565-1572, 1962.

Knight, M. D., Stratigraphy and anisotropy of magnetic susceptibility of the Toba ignimbrites North Sumatra, M.S. thesis, 279 pp., Univ. of Hawaii, Manoa, 1985.

Kuno, H., T. Ishikawa, Y. Katsui, Y. Yago, M. Yamasaki, and S. Taneda, Sorting of pumice and lithic fragments as a key to eruptive and emplacement mechanism, Jpn. J. Geol. Geogr., 35, 223-238, 1964.

Larson, E. E., M. Ozima, M. Ozima, T. Nagata, and D. Strangway, Stability of remanent magnetization of igneous rocks, Geophys. J. R. Astron. Soc., 43, 263-292, 1969.

Ledbetter, M., and R. S. J. Sparks, The duration of large-magnitude silicic eruptions deduced from graded bedding in deep-sea tephra layers, Geology, 7, 240-244, 1979.

Lipman, P. W., Mineral and chemical variations within an ash-flow sheet from Aso caldera southwestern Japan, Contrib. Mineral Petrol., 16, 300-327, 1967.

Mimura, K., and N. S. MacLeod, Source directions of pumice and ash deposits near Bend, Oregon, Geol. Soc. Am. Abstr. Programs, 10, 137, 1978.

Ninkovich, D., N. J. Shackleton, A. A. Abdel-Monem, J. D. Obradovich, and G. Izett, K-Ar age of the late Pleistocene eruption of Toba, North Sumatra, Nature, 276, 574-577, 1978a.

Ninkovich, D., R. S. J. Sparks, and M. T. Ledbetter, The exceptional magnitude and intensity of the Toba eruption, Sumatra: An example of the use of deep-sea tephra layers as a geological tool, Bull. Volcanol., 41, 286-298, 1978b.

Nishimura, S., E. Abe, T. Yokoyama, S. Wirasantosa, and A. Dharma, Danau Toba--The outline of Lake Toba, North Sumatra, Indonesia, Paleolimnol. Lake Biwa Japan Pleistocene, 5, 313-332, 1977.

Nishimura, S., E. Abe, J. Nishida, T. Yokoyama, A. Dharma, P. Hehanussa, and F. Hehuwat, A gravity and volcano-stratigraphic interpretation of the Lake Toba region, North Sumatra, Indonesia, Tectonophysics, 109, 253-272, 1984.

Nye, J. R., Physical Properties of Crystals, 322 pp., Oxford University Press, New York, 1969.

Ozima, M., and M. Ozima, Origin of thermoremanent magnetization, J. Geophys. Res., 70, 1363-1369, 1965.

Owens, W. H., Mathematical model stuties on factors affecting the magnetic anisotropy of

deformed rocks, Tectonophysics, 24, 115-113, 1974.
Ragan, D. M., and M. F. Sheridan, Compaction of the Bishop Tuff, California, Geol. Soc. Am. Bull., 83, 95-105, 1972.
Ramsay, J. G., Folding and Fracturing of Rocks, pp. 1-568, McGraw-Hill, New York, N.Y., 1967.
Rees, A. I., The use of anisotropy of susceptibility in the estimation of sedimentary fabric, Sedimentology, 4, 257-271, 1965.
Rhodes, R. C., and E. I. Smith, Distribution and directional fabric of ash flow sheets in the Northwestern Mogollon Plateau, New Mexico, Geol. Soc. Am. Bull., 83, 1863-1868, 1972.
Ross, C. S., and R. L. Smith, Ash-flow tuffs: Their origin, geologic relations and identification, U.S. Geol. Surv. Prof. Pap., 366, 1-81, 1961.
Ryan, W. B. F., Stratigraphy of the Late Quaternary sediments in the Eastern Mediterranean, in The Mediterranean Sea, edited by D. J. Stanley, Dowden, Hutchinson, and Ross, pp. 149-169, Stroudsburg, Pa., 1972.
Schmincke, H.-U., and D. A. Swanson, Laminar viscous flowage structures in ash flow-tuffs from Gran. Canaria, Canary Islands, J. Geol., 75, 641-664, 1967.
Smith, J. D., and J. H. Foster, Geomagnetic reversal in Brunhes normal polarity epoch, Science, 163, 565-567, 1969.
Smith, R. L., Ash-flow magmatism, in Ash-Flow Tuffs, edited by C. E. Chapin and W. E. Elston, Spec. Pap. Geol. Soc. Am., 180, 5-27, 1979.
Sparks, R. S. J., Stratigraphy and geology of the ignimbrites of Vulsini Volcano, Central Italy, Geol. Rundsch., 64, 497-523, 1975.
Sparks, R. S. J., Grain size variation in ignimbrites and implications for the transport of pyroclastic flows, Sedimentology, 23, 147-188, 1976.
Sparks, R. S. J., S. Self, and G. P. L. Walker, Products of ignimbrite eruptions, Geology, 1, 115-118, 1973.
Stone, D. B., Anisotropy of magnetic susceptibility measurements on a phonolite and on a folded metamorphic rock, Geophys. J. R. Astron. Soc., 7, 375-390, 1963.
Suzuki, K., and T. Ui, Grain orientation and depositional ramps as flow direction indicators of a large-scale pyroclastic flow deposit, Japan, Geology, 10, 429-432, 1982.
Taira, A., and B. R. Lienert, The comparative reliability of magnetic, photometric and microscopic methods of determining the orientations of sedimentary grain, J. Sediment. Petrol., 49(3), 759-772, 1979.
Tukey, J. W., Comments and suggestions on note 1 by Chayes, Earth Sci. Panel Rev. Group, Comment (1A) mimeo. rept., pp. 5, 1954.
Uyeda, S., M. D. Fuller, J. C. Belshe, and R. W. Girdler, Anisotropy of magnetic susceptibility in rocks and minerals, J. Geophys. Res., 68, 279-291, 1963.
van Bemmelen, R. W., The volcano-tectonic origin of Lake Toba (North Sumatra), Ing. Ned. Indie, 6, 126-140, 1939.
van Bemmelen, R. W., The geology of Indonesia, in General Geology of Indonesia and Adjacent Archipelagos, 732 pp., Government Printing Office, The Hague, 1949.
Verhoogen, J., The origin of the thermoremanent magnetization, J. Geophys. Res., 64, 2441-2449, 1959.
Walker, G. P. L., Origin of coarse lithic breccias near ignimbrite source vents, J. Volcanol. Geotherm. Res., 25, 157-171, 1985.
Walker, G. P. L., and L. Wilson, Lateral variations in the Taupo ignimbrite, J. Volcanol. Geotherm. Res., 18, 117-133, 1983.
Walker, G. P. L., S. Self, and P. C. Froggatt, The ground layer of the Taupo ignimbrite: A striking example of sedimentation from a pyroclastic flow, J. Volcanol. Geotherm. Res., 10, 1-11, 1981.
Westerveld, J., On the origin of acid volcanic rocks around Lake Toba, North Sumatra, Proc. K. Ned. Akad. Wet., Ser. B, Phys. Sci. 43, 1-51, 1947.
Westerveld, J., Quaternary volcanism on Sumatra, Geol. Soc. Am. Bull., 63, 561-594, 1952.
Wilson, C. J. N., and G. P. L. Walker, The Taupo eruption, New Zealand, Philos. Trans. R. Soc. London, Ser. A., 314, 199-228, 1985.
Wolff, J. A., and J. V. Wright, Rheomorphism of welded tuffs, J. Volcanol. Geotherm. Res., 10, 13-34, 1981.
Wright, J. V., The Rio Caliente ignimbrite: Analysis of a compound inteaplinian ignimbrite from a major late Quaternary Mexican eruption, Bull. Volcanol., 44, 189-212, 1981.
Wright, J. V., and G. P. L. Walker, The ignimbrite source problem: Significance of a co-ignimbrite lag-fall deposit, Geology, 5, 729-732, 1977.
Wright, J. V., and G. P. L. Walker, Eruption transport and deposition of ignimbrites: A case study from Mexico, J. Volcanol. Geotherm. Res., 9, 111-131, 1981.
Yokoyama, I., Volcanic calderas and meteorite craters with the special relation to their gravity anomalies, J. Fac. Sci., Hokkaido Univ., Ser. 7, 2, 37-47, 1963.
Yokoyama, S., Mode of movement and emplacement of Ito pyroclastic flow from Aira Caldera, Japan, Sci. Rep. Tokyo Kyoiku Daigaku, 12, 17-62, 1974.
Yokoyama, T., S. Nishimura, E. Abe, Y. Otofuji, T. Ikeda, S. Suparka, and A. Dharma, Volcano-, magneto-, and chrono-stratigraphy and geologic structure of Danau Toba, Sumatra, Indonesia, in Physical Geology of Indonesian Island Arcs, edited by S. Nishimura, pp. 122-143, Kyoto University, 1980.
Zijderveld, J. D. A., A.f. demagnetization of rocks: Analysis of results, in Developments in Solid Earth Geophysics, vol. 3, Methods in Paleomagnetism, edited by D. W. Collinson, R. M. Creer, and S. K. Runcon, pp. 254-286, Elsevier, New York, 1967.

J. F. Diehl, Department of Geology and Geological Engineering, Michigan Technological University, Houghton, MI 49931.
B. B. Ellwood, Department of Geology, University of Texas at Arlington, Arlington, TX 76019.
M. D. Knight and G. P. L. Walker, Hawaii Institute of Geophysics, University of Hawaii, 2525 Correa Road, Honolulu, HI 96822.

(Received November 27, 1985:
revised April 7, 1986:
accepted May 9, 1986.)